Naval Aerospace Medical Research Laboratory

NAMRL Monograph 48

DOES VERGENCE INFLUENCE THE VESTIBULO-OCULAR REFLEX IN HUMAN SUBJECTS ROTATING IN THE DARK?

A. B. Fajardo

DTIC QUALITY INSPECTED 4

19970203 098

Naval Aerospace Medical Research Laboratory
51 Hovey Road
Pensacola, Florida 32508-1046

Approved for public release; distribution unlimited.

Reviewed and approved 21 Aug 96

L. H. FRANK, CAPT, MSC USN
Commanding Officer

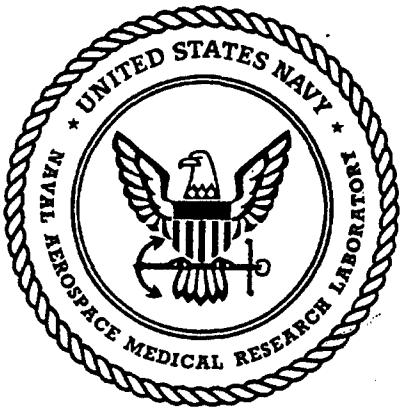

This research was sponsored by the Naval Medical Research and Development Command under work units 61153N MR04101.00F-7303 and 61153N MR04101.00G-7405.

The views expressed in this article are those of the authors and do not reflect the official policy or position of the Department of the Navy, Department of Defense, nor the U.S. Government.

Volunteer subjects were recruited, evaluated, and employed in accordance with the procedures specified in the Department of Defense Directive 3216.2 and Secretary of the Navy Instruction 3900.39 series. These instructions are based upon voluntary informed consent and meet or exceed the provisions of prevailing national and international guidelines.

Trade names of materials and/or products of commercial or nongovernment organizations are cited as needed for precision. These citations do not constitute official endorsement or approval of the use of such commercial materials and/or products.

Reproduction in whole or in part is permitted for any purpose of the United States Government.

NAVAL AEROSPACE MEDICAL RESEARCH LABORATORY
51 HOVEY ROAD, PENSACOLA, FL 32508-1046

NAMRL Monograph 48

DOES VERGENCE INFLUENCE THE VESTIBULO-OCULAR REFLEX IN HUMAN SUBJECTS ROTATING IN THE DARK?

A. B. Fajardo

Approved for public release; distribution unlimited.

DOES VERGENCE INFLUENCE THE VESTIBULO-OCULAR REFLEX IN HUMAN SUBJECTS ROTATING IN THE DARK?

by
Ann B. Fajardo

Thesis submitted to the Faculty of the Virginia Polytechnic Institute and State University in partial fulfillment of the requirements for the degree of

MASTER OF SCIENCE
IN
ENGINEERING MECHANICS

APPROVED:

J. Wallace Grant, Chair

L. Glenn Kraige

Brian J. Love

July 15, 1996
Blacksburg, Virginia

Keywords: Vergence, Vestibulo-ocular reflex, Eye movements

DOES VERGENCE INFLUENCE THE VESTIBULO-OCULAR REFLEX IN HUMAN SUBJECTS ROTATING IN THE DARK?

by
Ann B. Fajardo
J. Wallace Grant, Chairman
Department of Engineering Science and Mechanics

ABSTRACT

In recent experiments involving acceleration stimuli, researchers instructed subjects to focus on a visual target while measuring the vestibulo-ocular reflex (VOR) in one eye. These experiments showed conclusively that the VOR is influenced by target distance. We, on the other hand, were interested in investigating the VOR of subjects accelerated in complete darkness. Specifically, we wished to determine the subject's vergence point, which cannot be accomplished using data obtained from only one eye. Hence, a binocular eye-tracking system that works in the dark was required. In the experiment described in this thesis, the subject was rotated in the dark on NAMRL's Coriolis Acceleration Platform. The position of each pupil center was tracked and recorded by two helmet-mounted infrared cameras connected to a computer-controlled data acquisition system. The position data were used to calculate the angles through which the eyes rotated, and then trigonometric principles were applied to construct the line of sight for each eye for any moment in time; the intersection of these two lines is the vergence point. With the NAMRL binocular eye-tracking system, an accelerating subject's vergence point can accurately be determined if it is less than 1.5 meters away. The vergence data obtained from this experiment suggest that vergence distance does not exclusively drive the VOR in the dark.

ACKNOWLEDGMENTS

This thesis is the product of work that was possible thanks to the professional and personal contributions of many people to whom I am deeply grateful.

In particular I would like to express my appreciation to

Dr. J. Wallace Grant, for his guidance and patience.

Lt. Brian L. Luke, for writing virtually all the LabVIEW code without which the experiment would certainly have been impossible. I am also grateful for the numerous occasions when he let me pick his brain and for making work fun throughout the course of this investigation.

Dr. Anil Raj, my co-experimenter, for his many long hours of hard work.

Dr. Fred E. Guedry, for being so willing to share his expertise in the field of vestibular response and for his undying devotion to research. His ideas initiated most of this work.

The technical team at the Naval Aerospace Medical Research Lab (NAMRL): Frank Thrasher, Phil Wolfe, Don Joffrion, Mike Hayden, Efrain Molina, and Joe Lloyd for their hard work in getting the experiment to run smoothly and safely.

The rest of the crew at NAMRL: whether they did or did not directly contribute to this project, they made my stay there a pleasure.

The following NAMRL funds supported this research: "Psychophysical and Neurophysiological Approaches to the Dynamics of Spatial Disorientation" (Work number 0601153N MR04101.00F-7303 [Code 413] Accession DN243516) and "Virtual Environment Displays in Acceleration Environments" (Work number 0601153N MR04101.00G-7405 [Code 413] Accession DN244594).

TABLE OF CONTENTS

LIST OF FIGURES

CHAPTER 2

CHAPTER 4

CHAPTER 5

CHAPTER 6

CHAPTER 7

CHAPTER 8

APPENDIX B

APPENDIX C

LIST OF TABLES

CHAPTER 8

APPENDIX B

APPENDIX C

APPENDIX D

This page intentionally left blank.

CHAPTER 1

INTRODUCTION

The brain, vestibular system, muscles and eyes work in harmony, monitoring head motion to coordinate smooth body locomotion and to maintain equilibrium. Amazingly, the interplay is ceaseless, allowing us to perform everyday tasks such as reading street signs while driving past them, maintaining balance as we turn to talk to someone, and keeping our view of surroundings stable while jogging down the street. The body has had many years to perfect this motion control system and can respond quite accurately to the combination of stimuli generated by angular and linear motion. Nevertheless, the vestibular system, like any sensitive instrument, has its limitations, working ideally within a particular range of stimuli. When we are exposed to the high-speed transit of modern society, and worse, to virtual reality devices, the brain can become confused and relay faulty information to the body. The resulting disorientation can cause harmless motion sickness during a roller coaster ride or catastrophic accidents such as plane crashes. It is therefore worthwhile to study how the body responds to motion so that we may work to prevent the damaging effects of disorientation.

In this study we concentrate specifically on how the vestibular system, a set of organs located in the inner ear that work like angular and linear accelerometers, communicates with the eyes to keep our visual images fixed as we manoeuver about. Without the mechanism called the vestibulo-ocular reflex (VOR), which regulates the movements the eyes make to counter head motion, the view of our world would be similar to what we would obtain from a video camera. Consider the view from a video camera placed on the shoulder of someone walking down the street: The image blurs as the camera bounces up and down. The VOR prevents this image "shake" by continually correcting the position of the eyes during head motion.

Many researchers (Lansberg, Guedry & Graybiel, 1965; McGrath, 1990; Merfeld, 1990; Paige, 1989; Paige & Tomko, 1991; Sargent & Paige, 1991; Skipper & Barnes, 1989; Wearne 1993) have investigated the VOR in humans and animals while manipulating the motion stimulus, visual stimulus, subject awareness, etc. From these studies we know that the VOR is active in the dark even though there is no image to stabilize. In the absence of visual stimuli, does the brain set an imaginary point to gaze upon and if so, how does it influence the eye velocity response? We consider this question and describe a proposed mathematical model that correlates eye response with the vergence point, the point in space upon which a person gazes. The model is based on the premise that there is a preset (by the central nervous system) imaginary vergence point in the dark for the eye to track while the body rotates. In order to verify that supposition, we designed an experiment in which we rotated subjects in a light-proof chamber while recording their eye movements. This experiment is unique because we employed a binocular camera system to mon-

itor the position of both eyes in the dark and used that data to determine the subject's vergence point. We will describe the experiment in detail, explain the data collection method and the vergence calculations. Finally, we will present the results of the experiment and discuss how the data clarifies what we know about the VOR.

Note: In lieu of devoting a chapter exclusively to the literature search, the literature review is included in chapter 3 entitled "Vestibular Research" and throughout this thesis.

CHAPTER 2

THE VESTIBULAR SYSTEM AND THE VESTIBULO-OCULAR REFLEX

2.1 Introduction

Our ability to control our posture, maintain equilibrium, and move about in a coordinated manner is something we take for granted because it takes no conscious effort. This body control system involves a series of complex interactions that begins with the vestibular system. The vestibular organs, which function as a set of accelerometers, are able to detect any combination of linear and angular accelerations. The brain continuously receives and interprets signals from the vestibular system and communicates with the eyes and muscles, which then execute the appropriate response for body and visual control.

In this chapter, we describe the anatomy and mechanics of the vestibular system. We also discuss the vestibulo-ocular reflex, the interaction between the vestibular system and the eyes.

2.2 Coordinate System

Before we explore the vestibular system, it is helpful to understand the coordinate system used to describe head movements. The conventional physiological coordinate system is a right-handed set of orthogonal *xyz*-axes. The *x*- and *y*-axes comprise the horizontal plane; with the origin of the axes positioned at the head's center, the *x*-axis points towards the front of the head, and the *y*-axis points out the left ear. The vertical *z*-axis points straight up. We adhere to the right-hand rule to describe the directions of linear and angular accelerations (see Figure 2.1).

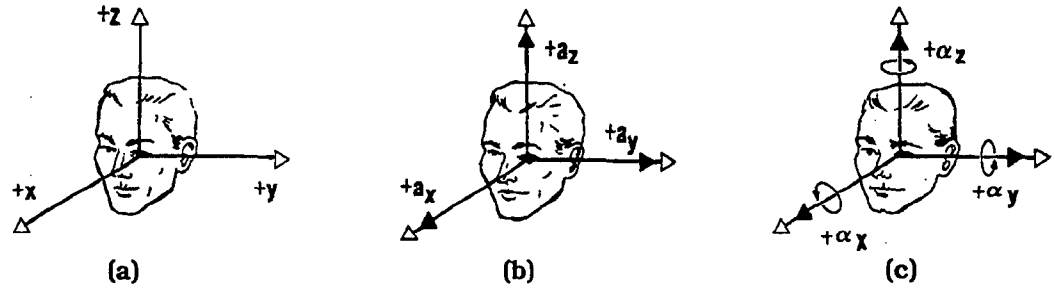

FIGURE 2.1. Coordinate system and convention for linear and angular accelerations. (a) Anatomical axes, (b) linear accelerations, and (c) angular accelerations. (From Gillingham & Wolfe, 1985.)

2.3 The Vestibular System

The vestibular apparatus is housed in the membranous labyrinth, which is located behind the ear within the temporal bone. The cochlea and the membranous labyrinth share a space within the bone and have interconnecting fluid systems. However, their functions are completely distinct; the cochlea is a hearing organ, whereas the labyrinth is devoted to sensing motion of the head.

The pea-sized membranous labyrinth depicted in Figure 2.2 is composed of three semicircular canals. These curved tubes, which are approximately orthogonal to each other, are conjoined and meet at the utricle, a sac-like structure. The utricle is connected to another similar sac-like structure called the sacculus; the two are collectively referred to as the otolith organs. The individual structures that make up the membranous labyrinth are interconnected and filled with a low viscosity fluid called endolymph. Perilymph fluid fills the space between the membranous labyrinth and its surrounding bony labyrinth. (Benson, 1982)

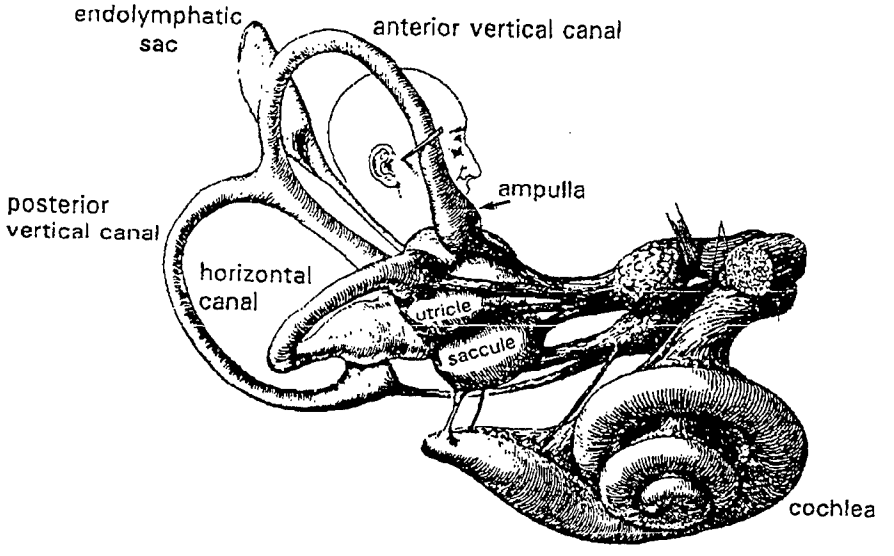

FIGURE 2.2. The vestibular organs. (From Hardy, 1934.)

2.3.1 The semicircular canals

Each semicircular canal contains a small bulged section called the ampulla (see Figure 2.3). The sensory cells are embedded within the crista ampullaris, the saddle-shaped ridge located within the floor of the

ampulla. Cilia, the hair-like projections of the sensory cells, extend into the cupula, a gelatinous mass that extends transversely across the ampulla and is connected to the perimeter of the ampulla's wall. The cupula serves as a diaphragm that prevents the free flow of the endolymph within the canal, yet it is sufficiently compliant to allow small displacements of the fluid during head rotation.

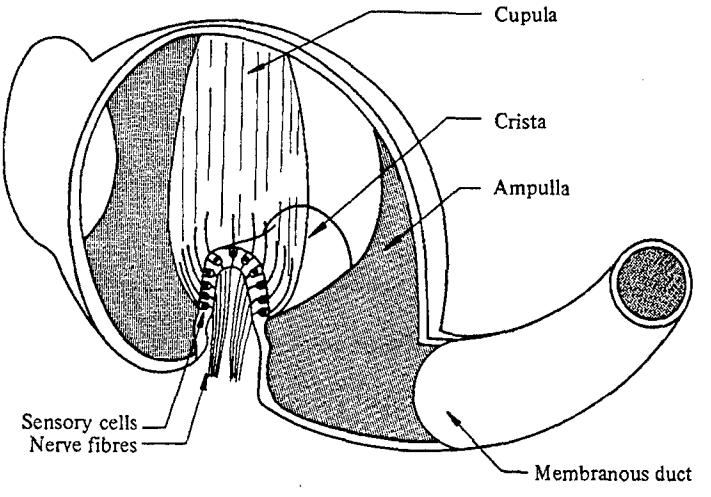

FIGURE 2.3. Cutaway of a semicircular duct's ampulla. (From Benson, 1982.)

The three canals, identified as anterior, posterior, and lateral, are situated in the head in three mutually orthogonal planes as shown in Figure 2.4(a). When the head is tilted downward 30 degrees (approximately the natural position of the head), the lateral canal is in the horizontal plane, and the anterior and posterior canals are vertical and lie at about 45 degrees from the *xz*- and *yz*-planes. Each semicircular canal responds to angular accelerations of the head in the plane of that canal. A head rotation about the axis of a canal displaces the endolymph fluid which causes the cupula and consequently, the cilia to deflect. The cilia deflection trig-

gers a signal to the brain, where the signal is interpreted as head rotation. (Benson, 1982)

2.3.2 The otoliths

The utricle and sacculus detect linear accelerations and provide information to the brain about the orientation of the head with respect to gravity (Wilson & Jones, 1979). The utricle and sacculus each contain a macula, a patch of sensory cells, along the inner wall. The principal planes of the utricular and saccular maculae are illustrated in Figure 2.4(b). The utric

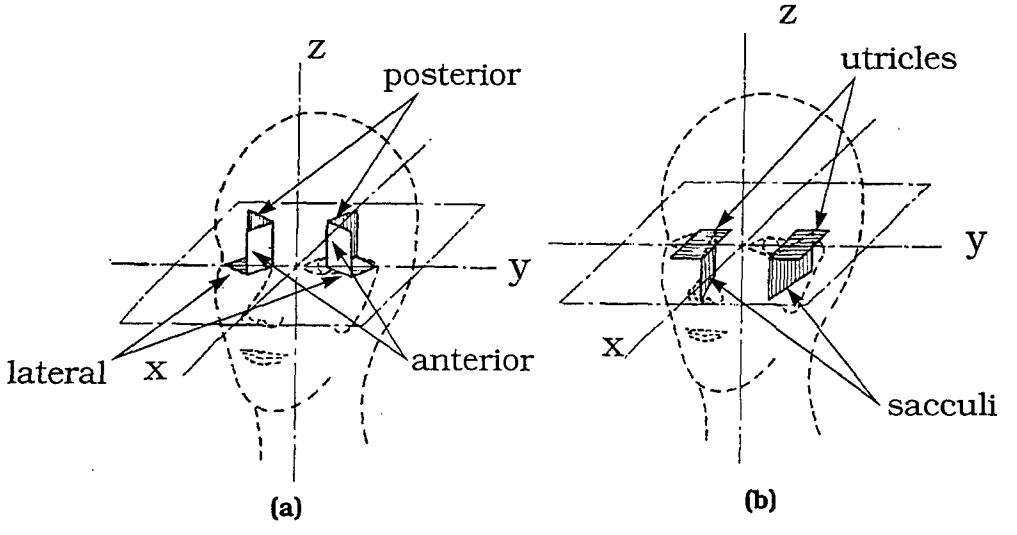

FIGURE 2.4. The orientation in the head of (a) the semicircular canals and (b) the utricles and sacculi. (From Benson, 1982.)

ular macula is approximately parallel to the lateral semicircular canal and is perpendicular to the nearly vertical saccular macula. Cilia extend from the sensory cells of the macula and are embedded in a gelatinous layer (see Figure 2.5). A rigid statoconial membrane composed of calcium carbonate crystals is attached to the surface of the gelatinous layer. The

cilia-gelatin-crystal membrane system deflects together when subjected to linear accelerations. The sensory cells of the otoliths, like those of the semicircular canals, relay a signal to the brain when triggered by cilia deflection; the sensory cells of the utricular macula respond primarily to horizontal head accelerations and those of the saccular macula respond primarily to vertical head accelerations. Because the action of gravity on a mass is indistinguishable from linear acceleration (Einstein, 1945), the otolith organs are also stimulated by static head tilt; linear accelerations and head tilt (which causes a change in the direction of gravity with respect to the head) generate the same type of cilia deflection. (Benson, 1982)

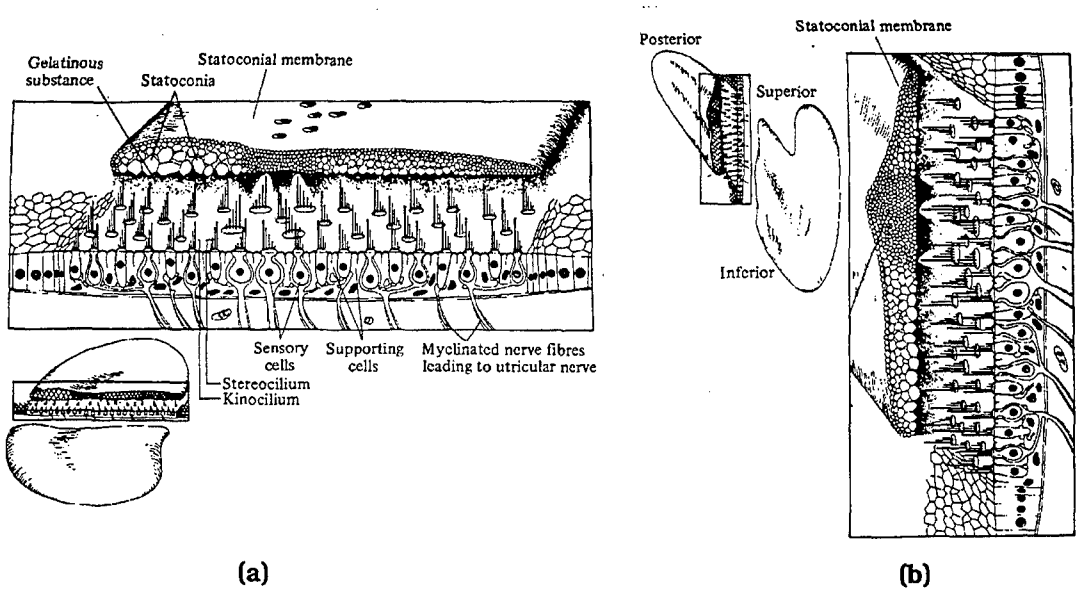

FIGURE 2.5. Cross sections of (a) the utricular macula and (b) the saccular macula. (From Benson, 1982.)

2.4 The Vestibulo-ocular Reflex

The vestibular system is only one tool the body utilizes to sense motion. Various mechanoreceptors dispersed throughout the body also provide information to the brain regarding the body's position. For example, a backward thrust into the back of one's seat produces a sense of forward acceleration.

In addition to vestibular signals and mechanoreceptor responses, the brain relies heavily on visual cues to maintain postural equilibrium. Indeed, people who lack functional vestibular systems can maneouver themselves quite well if provided with adequate visual cues. (Benson, 1982) In normal people, the vestibular system is intimately connected to vision. Most people have experienced the sensation of motion while sitting in a stationary car as an adjacent vehicle suddenly moves forward or backward. The vestibular system is not activated in this situation, but the peripheral vision provides motional cues that are strong enough to elicit a compelling sensation of motion in the direction opposite to that of the moving car. (Gillingham and Wolfe, 1985)

The visual and vestibular systems work interdependently; the brain uses visual as well as vestibular cues to stabilize the body and the vestibular system sends information to the eyes to stabilize the retinal image during head movements. (Benson, 1982) The vestibulo-ocular reflex (VOR) is the eyes' automatic compensatory response to head motion. For example, if the head rotates to the left, the eyes will rotate at an equal velocity and angle to the right. One can appreciate the vestibulo-ocular interaction by performing a simple exercise. As one waves a hand left and right in front of the face, the eyes can fix upon the hand when it moves at a slow veloc-

ity. As the velocity increases, however, the eyes cannot keep up and the image of the hand blurs. In contrast, if one oscillates one's head left and right as the hand remains fixed in front of the face, the image of the hand remains clear even at rapid head velocities. (Gillingham & Wolfe, 1985)

There are two types of VOR: The angular VOR (AVOR) is the response to angular head movements as described in the example above, and the linear VOR (LVOR) is the response to linear motion. Examples of motions that elicit the LVOR include riding an elevator or traveling straight ahead in a car while looking out the passenger side window. Virtually all natural human motions involve combinations of both linear and angular movements.

The VOR is more complex when the head is subjected to large amplitude displacements. The slow compensatory movement of the eyes is interrupted by a fast phase component, a saccade, during which the eyes move rapidly in the opposite direction. They then resume the slow compensatory movement. The alternating pattern of slow phase and fast phase eye velocities, referred to as nystagmus, is illustrated in Figure 2.6.

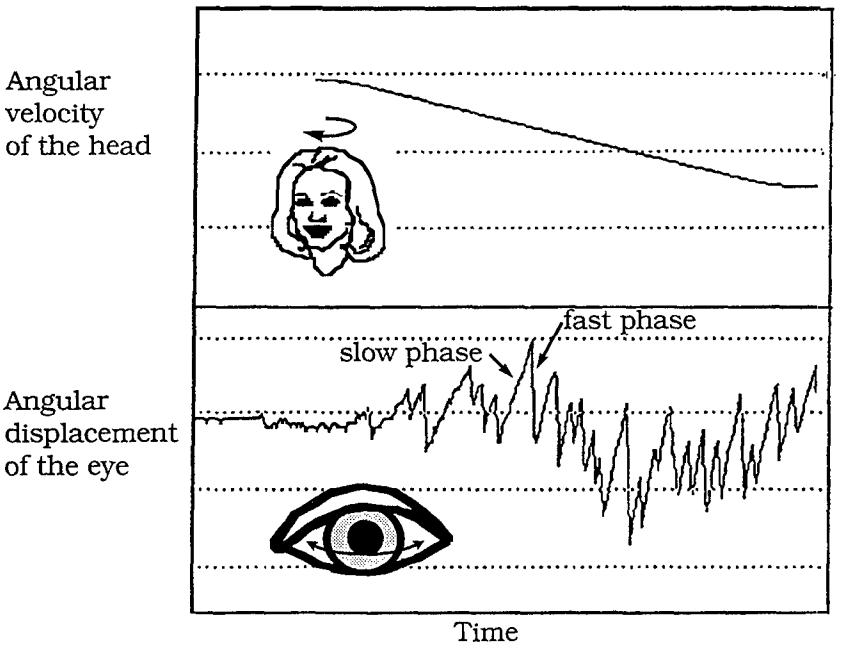

FIGURE 2.6. Nystagmus. The bottom graph shows the eye response to sustained rotation (the stimulus is shown in the top graph). Notice the alternating pattern of slow and fast phases.

2.5 Vestibular Response to Sustained Rotation

During natural head rotations, which are high speed and short in duration, the semicircular canal sensory response resembles that of a tachometer. The cupular deflection is proportional to the angular velocity of the head (see Figure 2.7[a]), even though head acceleration is the effective stimulus to the cupula (Naval Aerospace Medical Institue [NAMI], 1991). The canals transduce velocity by means of virtually instantaneous hydrodynamic integration of the head angular acceleration (Wilson & Jones, 1979). As a result, the turning sensation as elicited by the deflection of the cupula is accurate during and after the turn, and the reflexive eye velocity correctly compensates for head velocity.

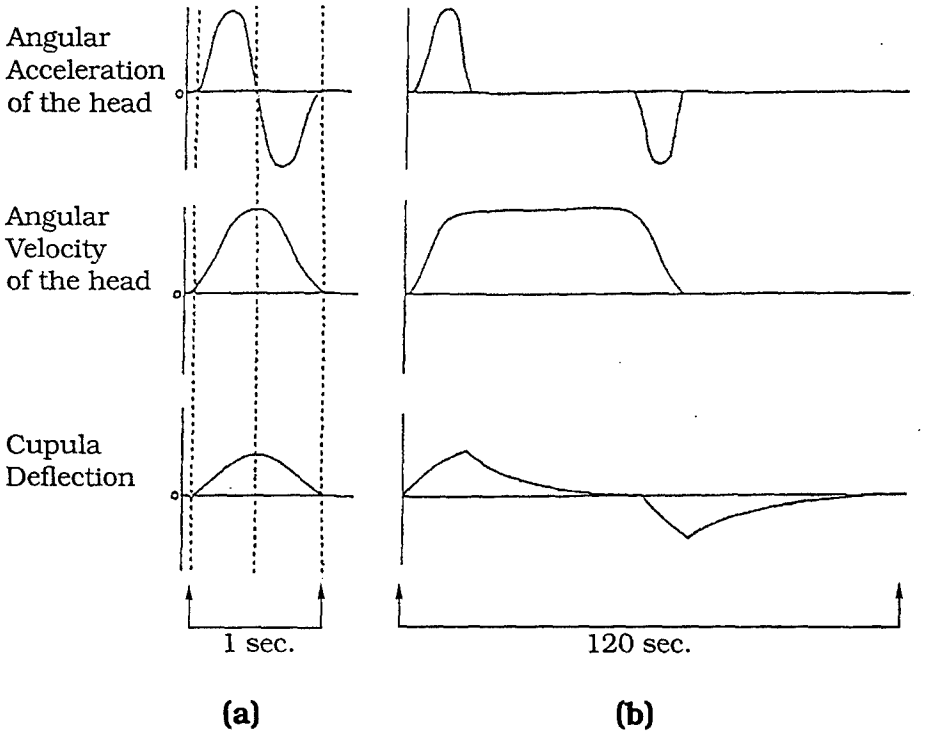

FIGURE 2.7. Comparison of cupula deflection during (a) a natural short turn and (b) a sustained turn of several revolutions. Notice that the cupula response resembles the angular velocity of the head during short duration motion (a), but resembles the angular acceleration of the head during sustained rotation (b). (From Naval Aerospace Medical Institute, 1991.)

However, during sustained rotation (an unnatural stimulus) such as is experienced during a centrifuge ride, the dynamic nature of the cupula causes false sensations of motion. During the angular acceleration of the head, the cupula deflects and correctly provides the sensation of rotation (NAMI, 1991). Shortly after the head reaches constant angular velocity, however, the restorative elasticity of the cupula causes it to return to its resting position and hence the sensory signal diminishes (see Figure 2.7[b]). As a result, the sensation of rotation diminishes until the rotating person feels stationary. When the head begins to experience the angular

deceleration after a period of constant angular velocity, the cupula begins to deflect from its resting position in the opposite direction. This causes the perception of rotation in the direction opposite to that of actual rotation that can persist for 30 to 40 seconds after the body has come to a stop. (Naval Aerospace Medical Institute [NAMI], 1991)

2.6 VOR Gain

The VOR gain is defined as the ratio of the eye movement (response) to head movement (stimulus); for our study, the gain is the ratio of the angular velocity of the eyes to the angular velocity of the head. Although the VOR gain typically provides an idea of how adequately the eyes respond to the stimulus (i.e., how well the eyes might track a target when the body is in motion), many factors affect it: pain, mental alertness, target distance, alcohol, and stimulus frequency, to name a few. For example, the VOR gain is 1.0 for a person who is spinning about a head-centered vertical axis tracks a point at infinity, but the gain increases as the target distance decreases. (Robinson, 1981)

CHAPTER 3

VESTIBULAR RESEARCH

3.1 Introduction

The ideal method to quantify vestibular sensory output directly is to record neural signals; unfortunately this requires surgery, making such data collection impractical for most human experiments involving motion stimuli. Alternatively, we can gain insight into vestibular function based on reports from experimental subjects regarding their perceptions of motion. However, such feedback is unreliable because it is dependent upon the subject's memory, experience, and state of awareness. (McGrath, 1990)

A convenient, quantitative measure of vestibular function, on the other hand, is the eye response to motion. B. J. McGrath comments:

> With a knowledge of the acceleration stimulus, the resulting nystagmus will give a measure of the combined function of the semi-circular canals, the otoliths, and the central oculomotor system. . . . By recording eye velocity and detecting and removing saccades from the eye velocity record, investigators are able to infer the net compensatory eye velocity command to the oculomotor system coming from the central vestibular system. (1990, p. 19)

Furthermore, eye movements are easy to record and can be measured non-invasively.

Much of what is known today about the vestibular system is derived from such eye motion research. Investigators have studied the vestibular response, in humans and other mammals, to stimuli encompassing virtually every type of motion (for a comprehensive reference list, please see section 1.9 of Boff & Lincoln, 1988). Here, we concentrate on outlining research associated with the AVOR and LVOR and how they might be related to vergence, the point in space where a person fixes his or her gaze.

3.2 Vergence and LVOR

Experimental evidence supports the notion that there is an apparent link between visual target distance and the LVOR. G. D. Paige (1989, 1991) showed that the amplitude of recorded eye motion depends on target distance for human subjects oscillating vertically; specifically, the amplitude of eye motion increases as target distance decreases. The same type of experiment performed on monkeys (Paige & Tomko, 1989) show results that agree with those of Paige (1989, 1991). Similarly, Skipper and Barnes (1989) demonstrated that the amplitude of eye motion increases as the distance to an earth-fixed target decreases in human subjects oscillating laterally (left and right) in the dark.

Both Paige (1989, 1991) and Skipper and Barnes (1989) also investigated the LVOR in the dark. Subjects gazed upon light source for a period of time while they translated vertically or laterally, and then continued imagining that visual target after it was extinguished. The researchers

found that in all cases, the eye velocity diminished after the target was extinguished; the eyes relax in the dark, shifting focus from the original target to somewhere beyond it.

Based on the results of his studies, Paige postulates that "vergence provides an internal signal of target distance which in turn modulates the LVOR. A finite 'dark vergence' might then provide the bias needed to generate the LVOR recorded during relaxed gaze in the dark." (Paige, 1989)

3.3 Combined AVOR and LVOR

We know that natural human motions are composed of combinations of both angular and linear accelerations. How do the canal and otolith signals integrate to produce eye responses under such stimuli? Various researchers have devoted their work towards answering this question.

We are primarily interested in the results of an experiment conducted by Lansberg, Guedry, and Graybiel (1965), in which they rotated subjects in the dark on a centrifuge. Each subject made several different runs, each time rotating counterclockwise at 84 deg/s (1.5 rad/s), but positioned in a different orientation with respect to the direction of rotation. The results from the forward-facing and backward-facing runs are the most intriguing. While facing the direction of motion, the maximum eye velocity was about -41 deg/s (-0.72 rad/s), but while traveling with back to motion, the eye velocity dropped to about -14 deg/s (-0.25 rad/s). Wearne (1993) and Merfeld (1990) reported similar findings from small-radius centrifuge experiments involving humans and squirrel monkeys, respectively. The difference in response is interesting because in these two positions, the semicircular canals retain the same orientation relative

to the plane of rotation, while the otoliths have different orientations with respect to the centripetal and tangential components of acceleration.

3.4 Unanswered Questions

Given the research described above, some questions arise. Is the LVOR responsible for the discrepancy between eye response to forward- and backward-facing centrifuge runs as reported by Lansberg, et al (1965)? That the eyes respond to motion in the dark is curious. If the VOR's function is to stabilize retinal images, why is it active even when in the absence of visual images? Is there a central nervous system-determined target distance in the dark as Paige (1989, 1991) suggests and does that target distance result in the difference between the forward- and backward-facing conditions? In the next chapter we consider such a "predetermined" target distance as the driving factor for the VOR and describe a mathematical model that defines the VOR with respect to target distance.

CHAPTER 4

VOR MODEL

4.1 Introduction

If eye velocity in the dark is driven by vergence, it is possible to derive a relatively simple mathematical model that describes eye position response to rotational acceleration. Indeed, Viirre, Tweed, Milner, and Vilis (1986) described such a model for subjects facing away from the center of rotation. In this chapter, we describe a model proposed by Guedry, Grant and McGrath (unpublished) that may explain the difference in eye response during forward-facing and backward-facing runs. This model was developed based on the hypothesis that vergence influences the VOR.

4.2 The Model

Consider a person traveling forward in a circular path with the head tangent to the path at all times, as depicted in Figure 4.1. What movements must the eyes make in order to track a point that is initially located directly in front of the face? Because the person is translating as well as rotating, both the AVOR and the LVOR drive the eye movements. As the

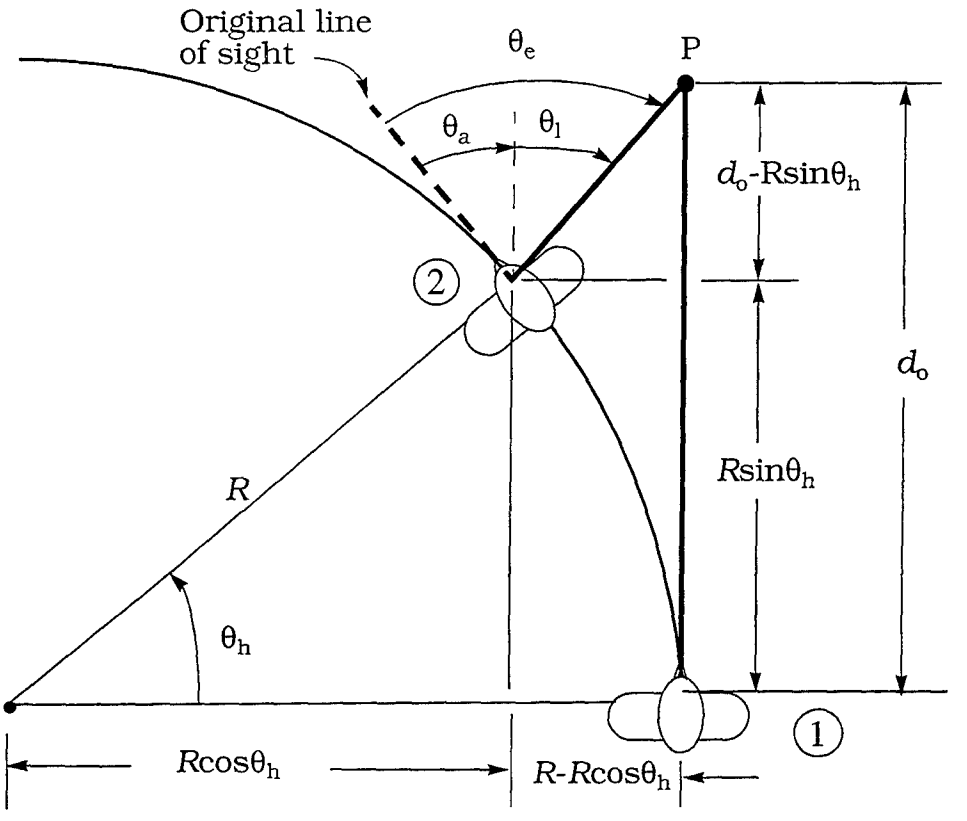

FIGURE 4.1. Forward-facing configuration. As the person travels from position 1 to position 2, the eyes must make an angular displacement θ_e in order to keep their gaze fixed on point P.

person travels through an arc of θ_h, the eyes rotate through an angle θ_e, which is equal to the sum of an AVOR component θ_a and a LVOR component θ_l.

$$\theta_e = \theta_a + \theta_l \qquad \text{(EQ 4.1)}$$

The AVOR component θ_a is equal in magnitude to the angle of head displacement θ_h, but opposite in sign.

$$\theta_a = -\theta_h \qquad \text{(EQ 4.2)}$$

Using trigonometry, we describe the angle θ_l in terms of the radius of the circular path R, the angular displacement of the head θ_h, and the original distance d_o from the person to the point of gaze,

$$\theta_l = -\text{atan}\left(\frac{R - R\cos\theta_h}{d_o - R\sin\theta_h}\right) \qquad \text{(EQ 4.3)}$$

If we substitute Equations 4.2 and 4.3 into Equation 4.1, we can quantify the total angular eye movement θ_e in terms of R, θ_h, and d_o, all measurable values.

$$\theta_e = -\theta_h - \text{atan}\left(\frac{R - R\cos\theta_h}{d_o - R\sin\theta_h}\right) \quad \text{Forward-facing} \qquad \text{(EQ 4.4)}$$

We can similarly describe the backward-facing scenario, which is depicted in Figure 4.2.

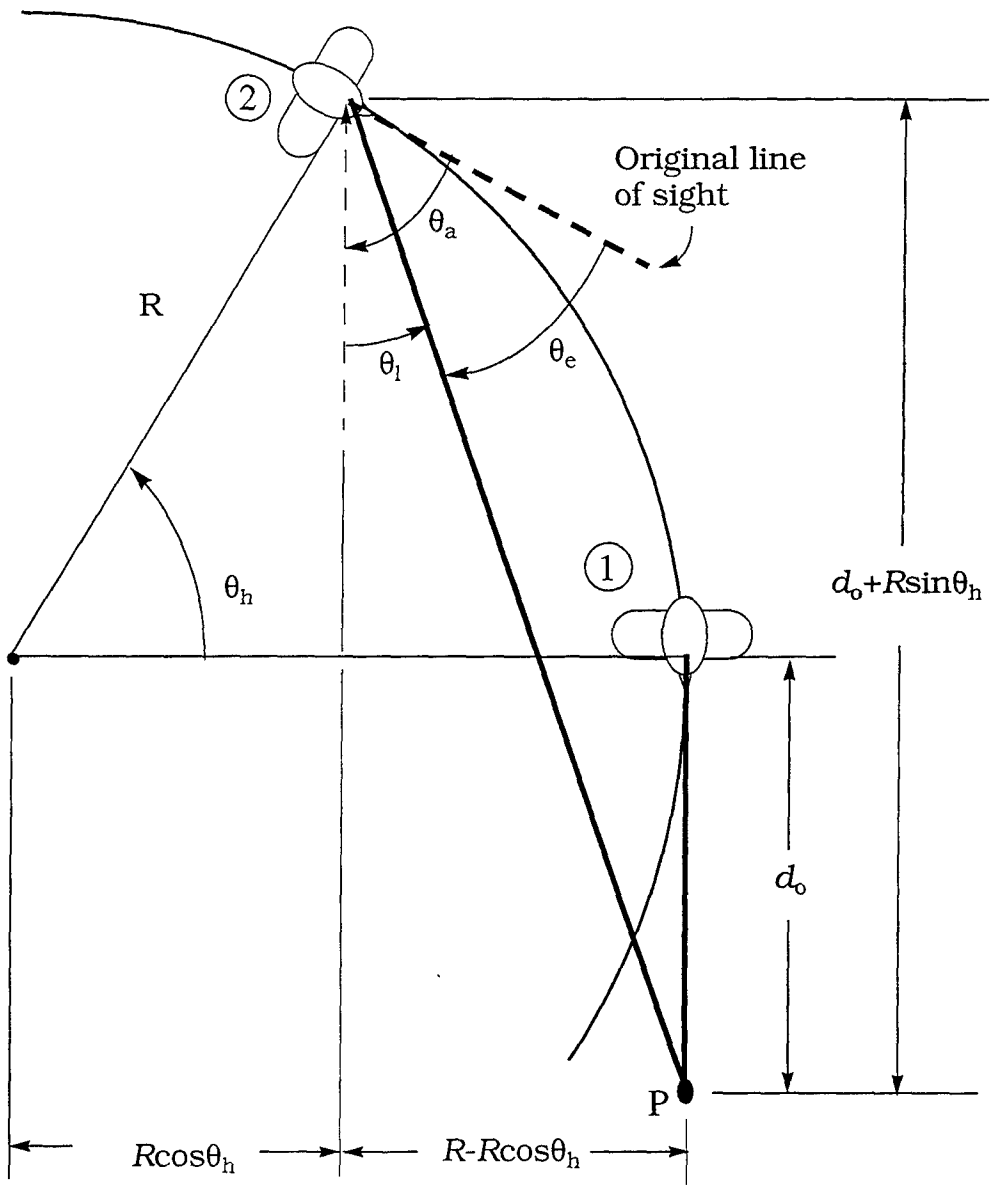

FIGURE 4.2. Backward-facing configuration.

Equations 4.1 and 4.2 are still applicable for the backward-facing condition. The expression for θ_l differs, however, due to the change in geometry. For the backward-facing condition, the equation for θ_l is as follows:

$$\theta_l = \text{atan}\left(\frac{R - R\cos\theta_h}{d_o + R\sin\theta_h}\right) \qquad \text{(EQ 4.5)}$$

Finally, for the backward-facing condition we describe the total angular displacement of the eye by combining Equations 4.1, 4.2, and 4.5.

$$\theta_e = -\theta_h + \text{atan}\left(\frac{R - R\cos\theta_h}{d_o + R\sin\theta_h}\right) \quad \text{Backward-facing} \qquad \text{(EQ 4.6)}$$

Notice that in the forward-facing case, the linear component adds to the angular component of eye motion, while in the backward-facing case, the linear component subtracts from the angular component of angular eye motion. Thus, the model accounts for the difference in angular velocity differences between the forward-facing and backward-facing conditions as reported by Lansberg, et al (1965).

This model describes how the eyes respond when a rotating person fixates on a stationary visual target. The model should apply equally well for a person rotating in the dark in the absence of visual cues if we suppose that d_o represents the preset dark vergence distance upon which he focuses.

4.3 MATLAB VOR Program

We can test the model by applying the known values from the Lansberg experiment into the above equations. Because the subjects were given no visual cues, the only unknown value is d_o. We will use the dark-focus distance (optical infinity) for the vergence distance : d_o = 20 ft (6.1 m). We know the radius R (6.2 m or 20.5 ft) and the angular acceleration of the head α_h (10.0 deg/s^2 or 0.175 rad/s^2), which we integrate once to find the angular velocity stimulus ω_h,

$$\omega_h = \alpha_h t \qquad \text{(EQ 4.7)}$$

and once again to find the angular displacement θ_h.

$$\theta_h = \frac{\alpha_h t^2}{2} \qquad \text{(EQ 4.8)}$$

We substitute the values for R and θ_h into Equations 4.4 and 4.6 for the time of acceleration (t = 0 to 8.4 s) and numerically differentiate θ_e for both the forward-facing and backward-facing conditions. In this fashion, we obtain the angular velocities of the eyes for both cases.

$$\omega_e = \frac{d\theta_e}{dt} \qquad \text{(EQ 4.9)}$$

We wrote a MATLAB program, incorporating the above equations and the Lansberg data, and plotted the angular displacement and angular velocity of the eyes as a function of time during acceleration of the apparatus. The program code is included in Appendix A. In writing the program, we assumed that the eye tracks the point until it has completed a 20 degree excursion and then resets its gaze to the original position (straight ahead).

We also incorporated a 0.075 s saccade, the component of nystagmus when the eye rapidly returns to the reset position. The graphs for the forward-facing and backward-facing cases are shown in Figures 4.3 and 4.4, respectively.

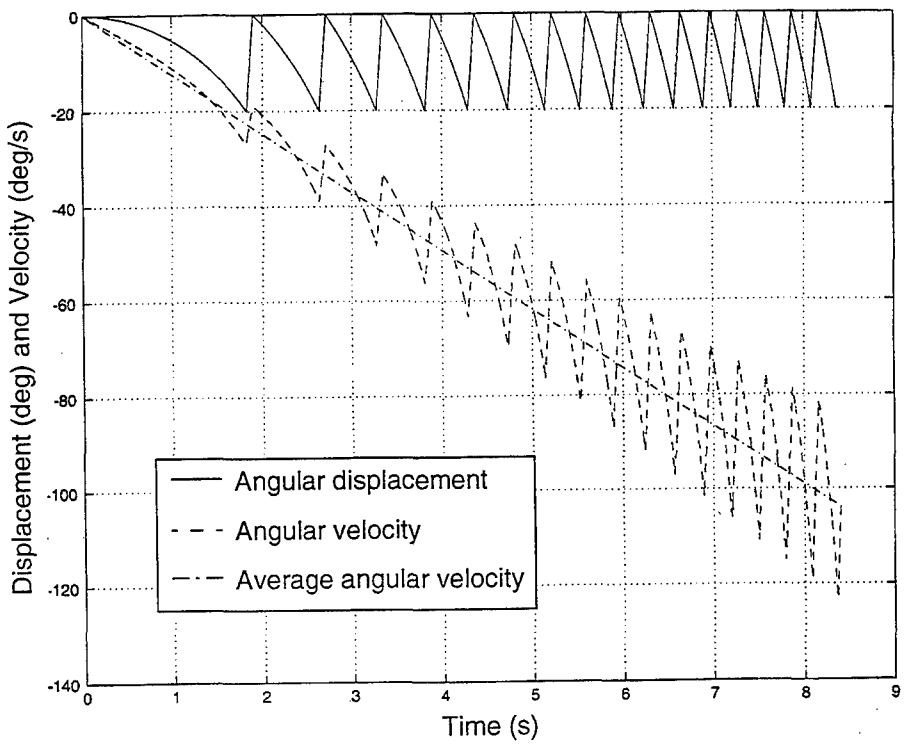

FIGURE 4.3. Angular displacement and velocity of the eye during acceleration of the subject in the forward-facing orientation.

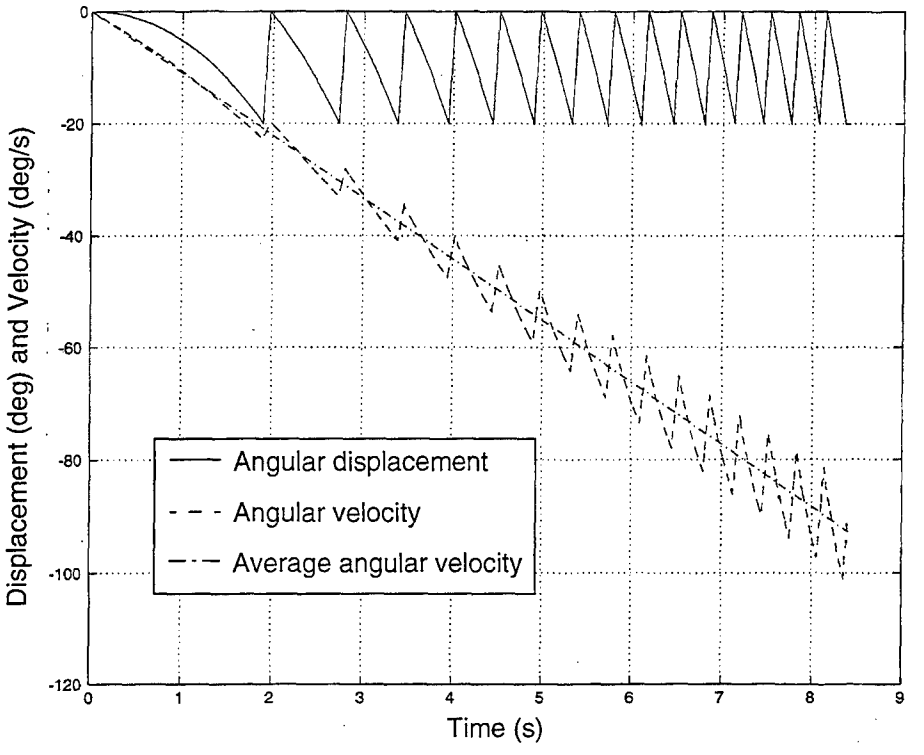

FIGURE 4.4. Angular displacement and velocity of the eye during acceleration of the subject in the backward-facing orientation

These figures show that the angular displacement of the eye as predicted by the model resembles that of true nystagmus (see Figure 2.6), and like eye angular velocity acquired from experimental data, the model-calculated angular velocity increases with head acceleration. The average angular velocity is represented by a line passing through the midpoints of each slow-phase velocity segment. Please note that when we speak of the model-calculated angular velocity throughout the remainder of this chapter, we refer to the average angular velocity.

Using the model, we compute the maximum angular velocity of the eyes to be approximately -105 deg/s (-1.83 rad/s) for the forward-facing condition and about -92 deg/s (-1.61 rad/s) for the backward-facing condition;

the model is successful in predicting a smaller angular velocity for the backward-facing condition as compared to the forward-facing condition. We may reduce the velocity magnitudes by multiplying them by some gain factor (the VOR gain is known to be less than 1.0 in the dark). How we apply gain to the results of the model is admittedly unclear because we do not know how the AVOR and LVOR interact. However, McGrath, Guedry, Oman, and Rupert (1995) formulated a canal model that predicts AVOR for subjects rotating about a vertical, head-centered axis (i.e., a pure rotational stimulus). The canal model, based on cupular mechanics, predicts an AVOR gain of 0.4 given the rotational acceleration and peak angular velocity stimulus of the Lansberg, et al. experiment. If we multiply both of the model-predicted peak angular velocities by a gain of 0.4, we then find that the predicted eye velocities for the forward-facing and backward-facing conditions are -42 deg/s and -37 deg/s, respectively. Although the calculated forward-facing eye velocity agrees with the Lansberg et al. results of -41 deg/s, the backward-facing eye velocity deviates from the -14 deg/s reported by Lansberg et al.

We wish to emphasize at this point that this model is presented as a proposed idea for explaining differences between forward- and backward-facing eye responses. Because we do not yet know enough about AVOR gain and LVOR gain, we cannot refine the model such that we can accurately predict eye velocity response.

4.4 Does Vergence Drive the VOR in the Dark?

This model is derived based on the premise that the VOR in the dark is driven by a preset vergence point. We would like to ascertain the validity of the basic assumption which can only be done experimentally. In the

next chapters we report how we measure eye movements and how we calculate vergence from eye motion data. Finally, we describe the experiment we designed to determine if vergence indeed is the driving force behind VOR.

CHAPTER 5

EYE MOTION MEASUREMENTS

5.1 Introduction

We measure eye motion to study vestibular function. Generally, experimenters record the position of the pupil and differentiate the position data to obtain eye velocity. In this chapter we describe the coordinate systems we use and then explain how we measure the position of the pupil.

5.2 Coordinate System

To simplify the kinematics of eye motion, we assume that the eye is a perfect sphere whose motion is composed only of pure rotations. For each eye, we define a head-fixed right-handed xyz-coordinate system, the origin of which is located at the center of the eye (see Figure 5.1[a]). The xy-plane is horizontal with respect to the head; the x-axis points out the front of the eye and the y-axis is directed toward the subject's left. The z-axis is the vertical axis, which points up through the top of the head. We then define the reference position of the eye to be where the center of the pupil coincides with the x-axis. The head-fixed coordinates of the pupil when it is in the reference position are $(r_e,0,0)$, where r_e is the radius of the eye.

We next define an eye-fixed $x'y'z'$-coordinate system such that, as the eye moves, the x'-axis always passes through the center of the pupil (see Figure 5.1 [b]).

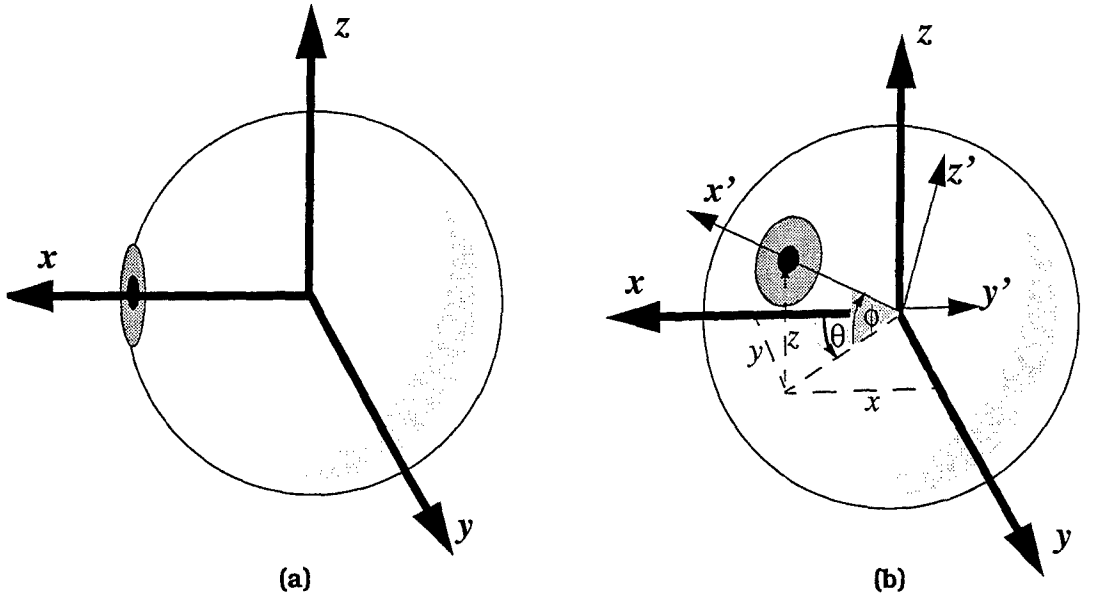

FIGURE 5.1. (a) Head-fixed and (b) Eye-fixed coordinate systems

The eye-fixed axes are located by rotating the head-fixed axes through an angle θ about the z-axis, and through an angle ϕ about the newly rotated y-axis. The x-, y-, and z-coordinates of the shifted pupil with respect to the head-fixed reference axes are described by the following equations (Moore, Haslwanter, Curthoys, and Smith, 1996):

$$x = r_e \cos\theta\cos\phi \qquad \text{(EQ 5.1)}$$

$$y = r_e \sin\theta\cos\phi \qquad \text{(EQ 5.2)}$$

$$z = -r_e \sin\phi \qquad \text{(EQ 5.3)}$$

However, we prefer to describe the position of each eye in terms of its horizontal and vertical angular displacements, θ and ϕ.

5.3 Eye Position Recording

Several techniques are available for measuring eye position. In electro-oculography (EOG), electrodes are placed near the eyes to record the potential difference between the retina and cornea of the eyes. EOG is relatively non-invasive, but tends to yield inaccurate vertical eye position information. Furthermore, erroneous data is recorded when the subject smiles, talks, and blinks, because the facial muscle activity produces electromagnetic signals which interfere with the EOG signal. The magnetic search coil technique is also commonly used because of the accuracy of the eye movement measurements. However, the subject is required to wear a contact lens which may cause discomfort or even damage to the eyes. (For more detail on these techniques, refer to Young, 1975)

For the experiment which we describe in chapter 7, we prefer to use a completely non-invasive method for measuring the pupil position. We employ an infrared binocular camera system to videorecord the image of each eye. Many researchers investigating eye movements have used a similar video-based eye-tracking system. However, to our knowledge, no one has videorecorded the eye movements of both eyes to determine vergence. Researchers who studied vergence were able to operate with a monocular system because they controlled the target distances in their experiments. However, because we wish to determine where a person is looking (the "target distance" is unknown) and resolve whether there is a naturally occurring vergence point, we require a binocular eye-tracking system. The helmet-mounted camera system we use is described below.

5.4 The Helmet-Mounted Binocular Camera System

Two COHU brand cameras are mounted to the helmet via an adjustable assembly, as depicted in Figure 5.2. In this configuration, the position of each camera is easily adjusted to optimize the size and focus of each eye on the screen. An infrared (IR) light-emitting diode (LED) attached to each camera illuminates the subject's eyes in the dark. The LEDs, which expose the eyes to wavelengths of 760 - 1400 nm, were deemed safe to use (McGrath, 1990). The image of the eye is reflected into the camera lens by a dichroic mirror tilted 45 degrees from vertical. The mirror extends from an arm attached to each camera. The camera lens is fitted with a high-pass KODAK Wratten gelatin filter (No. 87 C) which permits light with a wavelength of 800 nm or greater (IR spectrum) to pass into the camera.

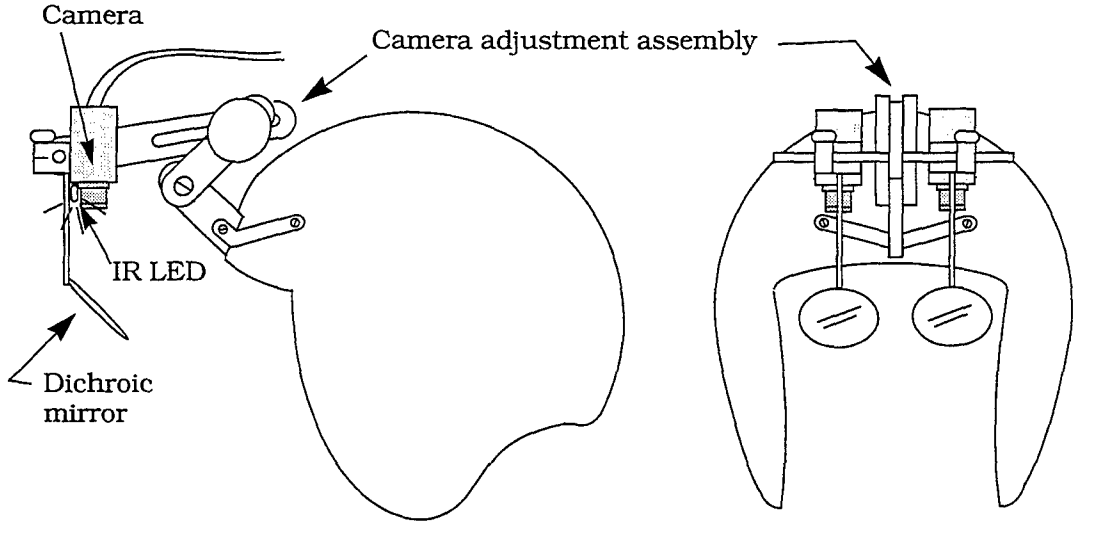

FIGURE 5.2. The infrared camera and adjustable helmet mount

5.5 ISCAN Eye Movement Monitoring System

The video image of the eye is sent to an IBM-compatible data acquisition computer (described in detail in chapter 7), which contains an ISCAN circuit board and software. The ISCAN system is a real-time digital processor that automatically tracks the center of a subject's pupil from a television image. (ISCAN, Inc., 1994) At a rate of 60 Hz, the ISCAN system detects the darkest part of the video eye image (the pupil), as defined by an operator-controlled threshold adjustment and locates the center. The system then sends an appended video image to a monitor; the operator can continuously view the image of the eye, as well as the thresholded pupil and the cross-hair that marks the pupil center. An example of the video eye image with the cross-hair is depicted in Figure 5.3.

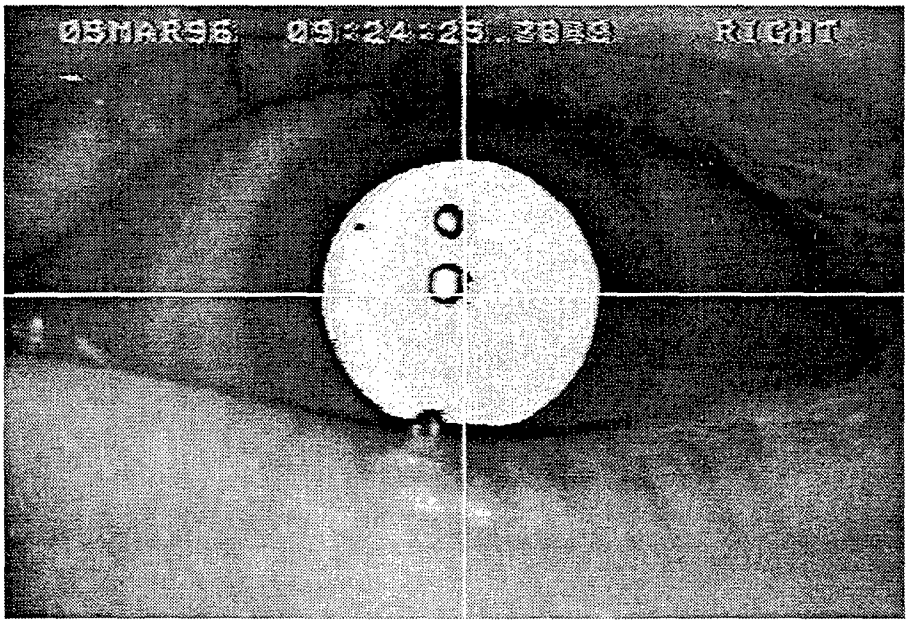

FIGURE 5.3. ISCAN video output for one eye. ISCAN marks the thresholded area (the pupil) in white. The crosshair indicates the center of the thresholded area. The two spots on the pupil are the direct and indirect (from the mirror) reflection of the infrared light source.

5.5.1 Output

The ISCAN system divides the video image into a 512 (horizontal) by 256 (vertical) pixel matrix. The location of the center of the pupil is sent to the computer's hard drive in terms of pixel coordinates, where (0,0) is located in the upper left-hand corner and (511,255) is located in the lower right-hand corner (see Figure B.1 in Appendix B).

5.5.2 Accuracy

The accuracy and range of eye movement that can be measured depends on the optical set-up and the size of the eye as seen on the monitor. Hence, the accuracy changes with each subject and with every camera adjustment. For our configuration, the average resolutions are approximately 0.3 deg/pixel (0.005 rad/pixel) for horizontal displacement and 0.6 deg/pixel (0.010 rad/pixel) for vertical displacement.

5.5.3 Calibration

Because we are interested in the angular position of the eye as described in section 5.2, rather than the pixel coordinates of the pupil center, we must perform a calibration in order to determine the conversion factors. A detailed description of the calibration procedure we used is located in Appendix B and an experimental verification of the calibration procedure (Test 1) is outlined in section 6.3 of chapter 6.

5.5.4 Limitations

Under ideal situations, the ISCAN system works very well. There are certain situations when ISCAN has trouble tracking the pupil, however. Very dark objects in the image such as shadows or black eyelashes confound

the system; ISCAN has difficulty isolating the pupil when the operator adjusts the threshold. ISCAN also has trouble tracking the pupils of subjects who have droopy upper eyelids or blink frequently.

Although ISCAN, Inc. (1994) recommends tilting the cameras to look up into the eyes of people with droopy eyelids, we found that this was not advisable. The image of the eye, particularly in the vertical dimension, distorts when the cameras are tilted. Therefore, we positioned the cameras as close to vertical as possible.

CHAPTER 6

VERGENCE

6.1 Introduction

Vergence (sometimes called convergence) describes the binocular eye movements required to fixate and focus upon an object. Vergence in an illuminated environment is well understood; if one looks at a chair 2 m away, then the vergence distance is 2 m. However, in the dark, vergence is more complex. Little is known about how the eyes operate in the dark. Without visual stimuli, where do the eyes look? In the experiment to be described in Chapter 7, our goal is to answer that question. We wish to determine where a person gazes while being rotated in the dark.

In this chapter, we describe how we calculate vergence from experimental eye position data. In order to do so, we must first assume that the point at which the subject is looking is also the point where he or she is focussed. We locate this point by extending a line from the center of each eye through the center of the pupils; the point at which these two lines intersect is the vergence point.

6.2 Calculating Vergence

To calculate vergence is simply an exercise in geometry and trigonometry. We measure the subject's interpupillary distance D and experimentally acquire the horizontal and vertical angular displacement for each eye: θ_r and ϕ_r (right eye), and θ_l and ϕ_l (left eye). With these variables we can determine the location of the vergence point VP (see Figure 6.1).

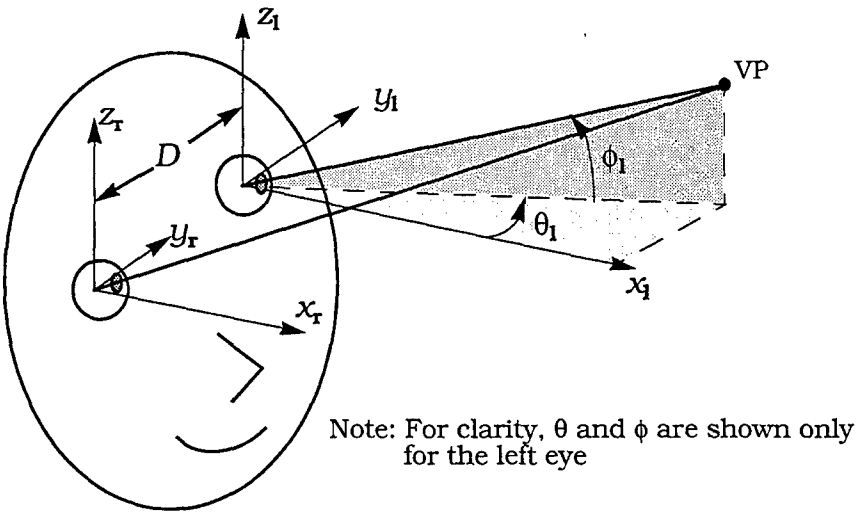

FIGURE 6.1. The vergence point VP. The location of VP is determined in terms of the interpupillary distance *D* and the horizontal and vertical angular displacements θ and φ of both the right and left eye.

We begin by projecting the vergence point VP onto the horizontal *xy*-plane, as shown in Figure 6.2(a). Consider the triangle that is formed by the two eyeball centers and the projected vergence point VP' (see Figure 6.2[b]). Knowing the values of θ_r, θ_l, and D, we can apply geometric principles to find the lengths of the other two sides of the triangle, R_r (the side emanating from the right eye) and R_l (the side emanating from the left eye), as well as the vergence angle γ formed by sides R_r and R_l.

We first solve for γ.

$$\gamma = 180 - (90 - \theta_r) - (90 + \theta_l)$$

$$\gamma = \theta_r - \theta_l \qquad \text{(EQ 6.1)}$$

We then solve for R_l using the law of sines:

$$R_l = \frac{D \sin(90 - \theta_r)}{\sin\gamma}$$

$$R_l = \frac{D \cos(\theta_r)}{\sin(\theta_r - \theta_l)} \qquad \text{(EQ 6.2)}$$

Finally, we apply the law of sines again to solve for R_r:

$$R_r = \frac{D \sin(90 + \theta_l)}{\sin\gamma}$$

$$R_r = \frac{D \cos(\theta_l)}{\sin(\theta_r - \theta_l)} \qquad \text{(EQ 6.3)}$$

For simplicity, we would like to describe the location of VP without reference to either eye. If we place a head-fixed coordinate system centered at a point midway between the eyes, as shown in Figure 6.2(c), we can describe the location of VP as (x_{VP}, y_{VP}, z_{VP}):

$$x_{VP} = R_l \cos(\theta_l) = R_r \cos(\theta_r) \qquad \text{(EQ 6.4)}$$

$$y_{VP} = \frac{D}{2} + R_l \sin(\theta_l) = R_r \sin(\theta_r) - \frac{D}{2} \qquad \text{(EQ 6.5)}$$

$$z_{VP} = R_r \tan(-\phi_r) = R_l \tan(-\phi_l) \qquad \text{(EQ 6.6)}$$

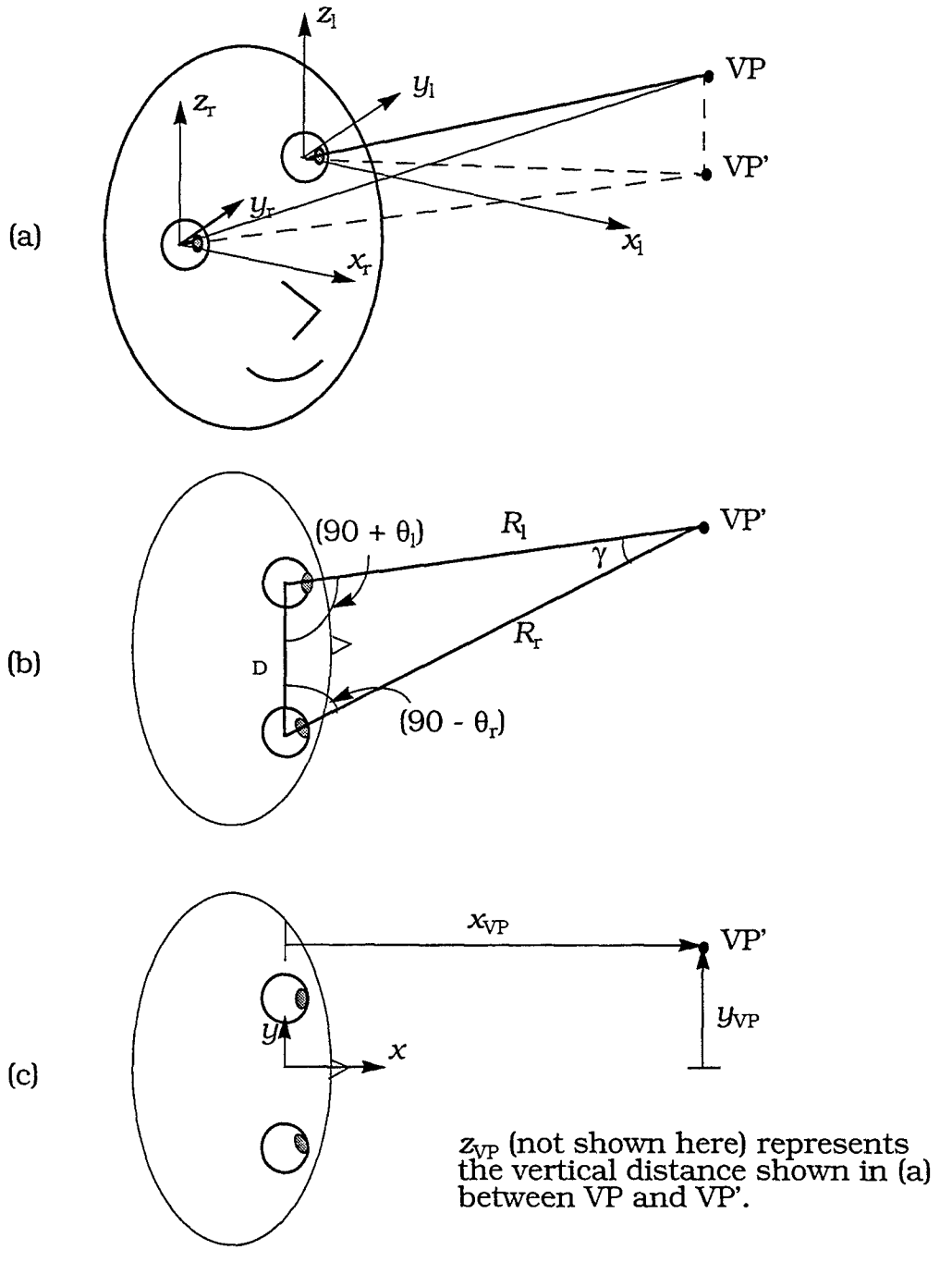

FIGURE 6.2. Locating the vergence point. (a) Vergence point VP is projected onto horizontal *xy*-plane, (b) Top view of the horizontal plane projection, (c) Coordinates of the projected vergence point VP' with respect to center of face.

6.3 Verification of Vergence Algorithm

To confirm the accuracy of our vergence algorithm, we performed three tests to ensure that the vergence algorithms were correct and to verify that the software was free of errors. We first had a subject sit in the stationary CORO capsule (see chapter 7) and went through the calibration procedure (refer to Appendix B). We then asked the subject to look at a number of points, the locations of which were measured with respect to the subject prior to recording data. We then compared manual calculations for the eye position and vergence distance with the results given by our software.

6.3.1 Procedure

Test 1

For the first test we simply applied the calibration factors to the eye position data recorded during the calibration procedure; that is, we ran the calibration data through the analysis program.

Test 2

We placed a yardstick in front of the subject's face, parallel to the subject's x-axis, and asked the subject to look at points on the yardstick at 5 inch (12.7 cm) intervals.

Test 3

With the subject seated outside the CORO, we directed the subject to look at points directly in front of the face at 6 in. (15.2 cm) intervals from 18 in. (45.7 cm) to 8 ft (2.4 m) away from the subject. Then we asked him or her to look at points at 1 ft (30.5 cm) intervals from 8 ft to 20 ft. (6.1 m) away.

The data from these tests are presented in Appendix C.

6.3.2 Accuracy of vergence calculations

The data from the tests confirm that the vergence algorithm is good. We were able to accurately (within 10% error) calculate the vergence distance when the subject looked at points less than 1.5 m away. The accuracy of the calculations decreases significantly when the subject looks at points beyond 1.5 m away because the eye makes smaller and smaller angular displacements to look further and further away. The accuracy of the calculations depends primarily on the sensitivity of the eye position measurements, yet it would be virtually impossible to distinguish when the eye looks at points beyond 3 m even with a perfect system. Although optical infinity is considered to be 6 m, even at 3 m the eyes are essentially parallel to each other.

CHAPTER 7

EXPERIMENT

7.1 Introduction

Our first aim was to duplicate the forward-facing and backward-facing stimuli as applied in the Lansberg et al. (1965) experiment to see if we found consistent eye velocity results. We applied an off-axis rotation stimulus to each of 28 subjects using the Coriolis Acceleration Platform (CAP) at the Naval Aerospace Medical Research Laboratory (NAMRL). Secondly, we wished to calculate the position of a subject's vergence point, as described in chapter 6, from the eye position data we experimentally measured.

The experiment described in this chapter is actually one part of a larger study performed at NAMRL.

7.2 Methods

7.2.1 Stimulus

We rotated each subject, either in a clockwise or counterclockwise direction, on NAMRL's centrifuge (described in section 7.2.2) at an angular acceleration of 10.0 deg/s^2 (0.175 rad/s^2) until the apparatus reached the

desired value for constant angular velocity. Half of the subjects were exposed to a constant angular velocity of 70.1 deg/s (1.2 rad/s), which corresponds to a maximum centripetal acceleration of 1g (9.8 m/s^2); the other half received a constant angular velocity of 99.2 deg/s (1.7 rad/s) which corresponds to a centripetal acceleration of 2g (19.6 m/s^2). Subjects remained at the constant angular velocity for 120 s, after which they were decelerated to a stop at a rate of -10 deg/s^2 (-1.2 rad/s^2). The angular velocity stimuli for both the 1g and 2g runs are illustrated in Figure 7.1. The radius of rotation was 21.5 ft (6.55 m), measured from the center of rotation to the center of the head.

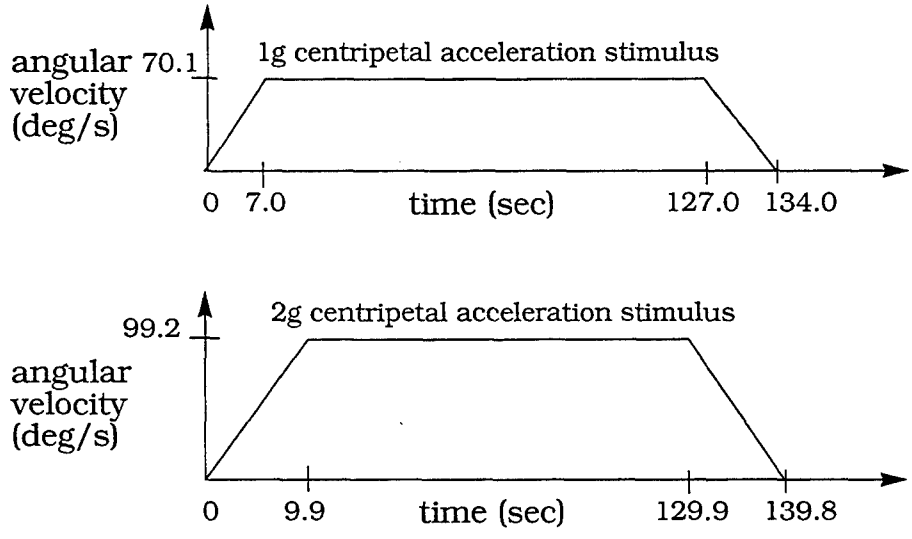

FIGURE 7.1. The angular velocity stimuli for 1g and 2g centripetal acceleration

Within each group (the 1g group and the 2g group), half of the subjects faced forward when spun in a counter-clockwise direction and the other half faced forward when spun in a clockwise direction (See Figure 7.2).

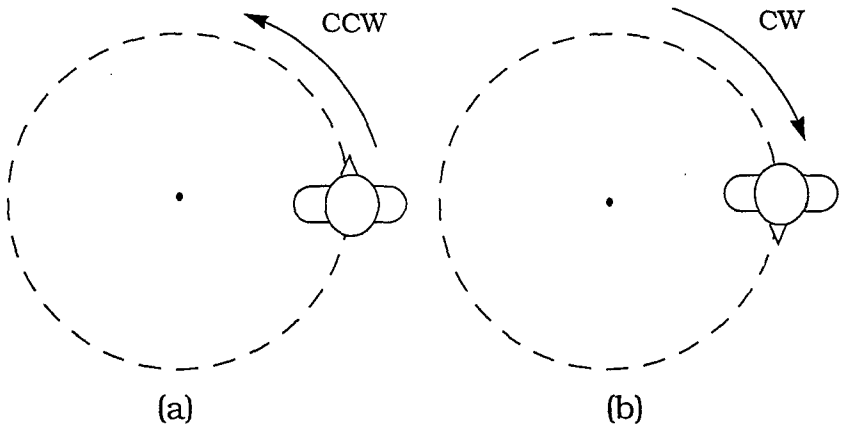

FIGURE 7.2. Forward-facing conditions. The subject in (a) is forward-facing when rotating counter-clockwise. The subject in (b) is forward-facing when rotating clockwise.

We gave all the subjects the backward-facing stimulus by rotating them in a direction opposite to that of their forward-facing condition.

7.2.2 Apparatus

The Coriolis Acceleration Platform

NAMRL's Coriolis Acceleration Platform (CAP) provided the rotational stimulus. The CAP, originally designed to study the effect of long term exposure to a rotating environment, consists of a large cylindrical room and a 14.6 m (48 ft) long track that rest on a pedestal (see Figure 7.3). A vertically mounted drive motor located inside the pedestal provides the rotational mechanical power. The lower base of the pedestal contains a slip-ring assembly for high-level power and control circuitry, as well as control and monitor velocity tachometers. The DC torque drive motor is

operated under closed-loop conditions. The overall rotary drive system is a velocity-mode power servomechanism. The electronic control of the velocity-time profile of angular motion is provided by a command signal which is linearly proportional to the desired angular velocity. The command signal is generated by a Wavetek model 275 function generator controlled by a Hewlett Packard 9826 computer, both located in the adjacent control room. A slip ring assembly, located directly above the center of the capsule, is used for the transmission of data to and from the control room. (Hixson & Anderson, 1966)

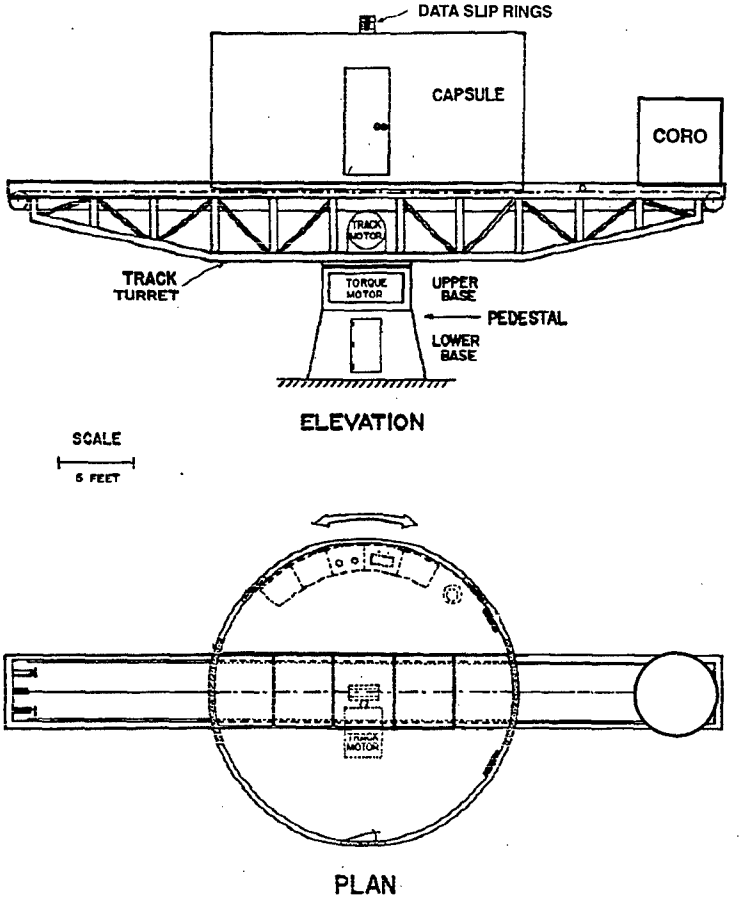

FIGURE 7.3. Sketch of the CORO on the Coriolis Acceleration Platform (CAP). (Adapted from Hixson & Anderson, 1966)

The subject was seated within the light-proof, cylindrically shaped CORO (short for Counter-Rotator) capsule, located at the end of the CAP's track. The CAP contains a second drive motor that allows a platform where the CORO is mounted to be linearly displaced along the radial axis of the track. The CORO is also capable of rotating about its own vertical axis while being simultaneously rotated by the CAP. However, for this experiment the CORO was simply fixed in place, clamped to the track arm. Prior to each run of the large-scale experiment, the CORO was rotated about its base and fixed in one of six orientations as illustrated in Figure 7.4. However, for this study, we are interested in only the tangential positions (90 and 270 degrees). The subject's seat and the helmet to which the eye cameras are attached are both fixed within the CORO.

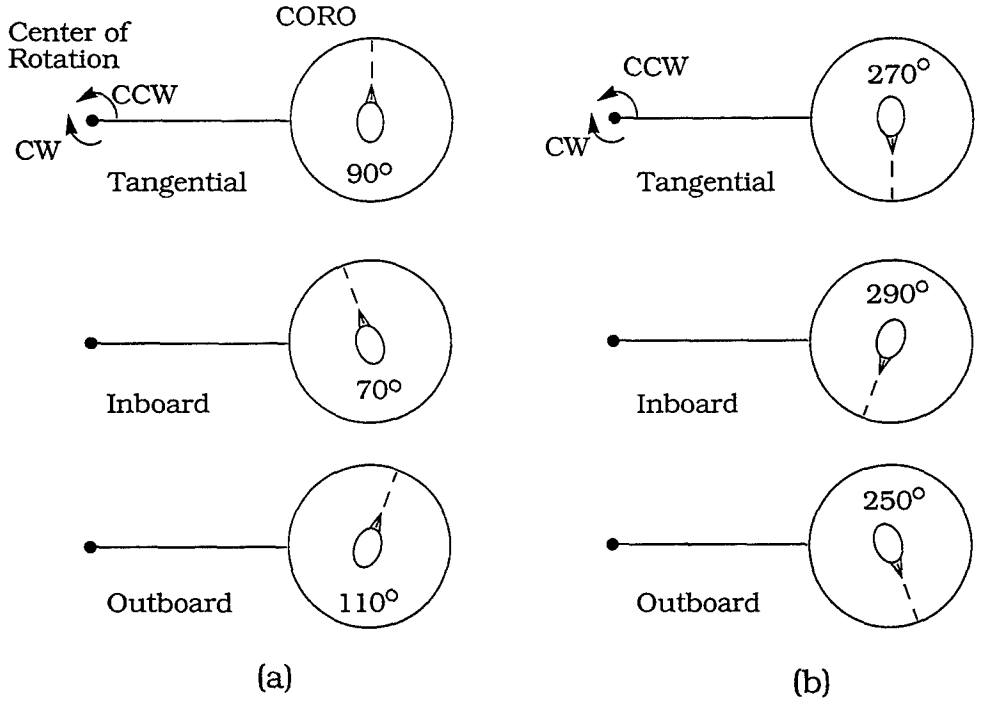

FIGURE 7.4. CORO positions. (a) Positions for the CCW-forward-facing condition; tangential (90 deg), inboard (70 deg), and outboard (110 deg). (b) Positions for the CW-forward-facing condition; tangential (270 deg), inboard (290 deg), and outboard (250 deg)

Restraints

Because the eye position recordings are sensitive to any movement of the subject with respect to the helmet, we took pains to immobilize the subject in his seat and within the helmet. The seat is equipped with a 5-point aerobatic harness and a shoulder restraint system that prevented the subject from moving in the seat during acceleration. We also used foam cushions to fill the space between the hip and the side of the seat. The helmet was designed to prevent head translation during acceleration. The helmet is attached to the seat by means of a C-clamp type mechanism which allowed us to compress the helmet against the subject's cheeks (see Figure 7.5); this clamp helped to prevent the head from shifting left or right. A modified aircraft oxygen mask (a piece was cut out to expose the nose and mouth) helped to keep the head from moving vertically. Additionally, the interior of the helmet was lined with an air bladder, similar to those used in blood pressure cuffs, to fill any space remaining in the helmet.

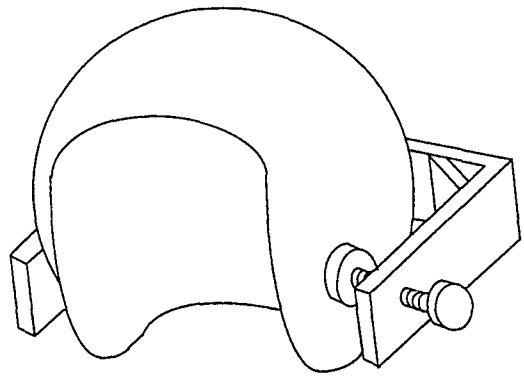

FIGURE 7.5. The C-clamp that supported and tightened the helmet. Although it is not shown, there is a bolt on the left side of the helmet identical to the one seen on the right.

Equipment on the CORO

Other equipment located within the CORO include the video calibration equipment, three linear accelerometers, a push button, an audio system, and a safety video camera. The video calibration system consists of a set of light-emitting diodes (LEDs) embedded in a curved screen along the front wall of the CORO (see Figure B.2 in Appendix B). The *x*- , *y*- and *z*-axis linear accelerometers (Columbia Research Laboratories, Inc. model SA-211200-10) are mounted to a cube located on the floor of the CORO just behind the seat.

The CORO is equipped with an audio system that allowed maintenance of verbal communication with the subject from the control room at all times. A microphone and speaker are located in the CORO capsule, and the helmet is also equipped with earphones and a microphone. As an added safety measure, we continuously observed the subject from the control room via a monitor connected to a video camera installed in the CORO. The infrared LEDs mounted to the helmet provide the illumination necessary to view the subject's face in the dark. We also installed a push button so that the subject could provide non-verbal feedback. A light bulb located in the control room illuminated when the subject pressed the button.

7.2.3 Subjects

Twenty eight healthy volunteers from the Pensacola Naval Air Station's flight school served as subjects for this study. They ranged in age from 22 to 28 years of age. Only one subject was female.

7.2.4 Experimental design

Each subject completed 6 runs; one pair of runs at the tangential position (one clockwise run and one counterclockwise run), one pair of runs at the inboard position, and one pair of runs at the outboard position. We randomized the run order for CORO position and direction of rotation. See Appendix D for each subject's run order.

7.2.5 Procedure

After briefing the subject and obtaining his or her consent (Appendix E contains a sample pre-experiment brief and consent form), we measured the interpupillary distance with a digital pupillometer. We then seated the subject inside the CORO, adding cushions to the seat if necessary to ensure that the top of the head contacted the top of the helmet. We adjusted the harness and shoulder restraint, placed the cushion between the hip and the chair, and strapped the subject's left (for the 90 deg runs) or right leg (for the 270 deg runs) to prevent it from drifting across and obstructing the safety camera during acceleration. With the subject well secured in the seat, we adjusted the helmet by clamping down the bolts on both sides of the head and then filling the air bladder. At this point, we measured the distance from the subject's eye to the screen as described in Appendix B. Lastly, we adjusted the position and focus of the eye cameras while checking the image on a video monitor, and then closed the capsule, leaving the subject in complete darkness.

We performed the calibration procedure as described in Appendix B while recording data. We began the first run, collecting data while the subject rotated in either a clockwise or counterclockwise direction. Because nystagmus sometimes persists for several seconds after actual motion has

stopped, we continued to record data for 60 seconds following the end of the run. After we verified that the subject experienced no motion sickness symptoms, we then proceeded with the second run, which was identical to the first, except that rotation was in the opposite direction. After the first pair of runs, we again confirmed that the subject felt able to continue, and then repositioned the CORO to the next orientation. In the meantime we turned on the overhead light in the CORO to prevent the eyes from becoming dark adapted, and allowed the subject to relieve the air bladder pressure if it caused discomfort. Before starting the next pair of runs, we asked the subject to pump the air bladder up again, and we extinguished the light. We proceeded to perform another calibration because the position of the eyes invariably changed during the waiting period. We ran the second and third pair of runs in the same fashion.

During the runs, the subject was asked to follow an auditory alerting task. We played an audio tape containing a series of computer generated tones. Each tone was of a random frequency and lasted either 0.8 s or 2.0 s in duration. The subject was to depress the push-button upon hearing the long tones, which were randomly dispersed and comprised approximately 40 percent of the tones. The purpose of the task was to keep the subject alert (the vestibular-ocular reflex is depressed when the subject feels drowsy) and to prevent conscious control of the eyes during the run (the subject was given no instructions as to where to direct his or her eyes).

7.2.6 Data acquisition system

All electronic data were collected by an IBM-compatible 486 DX2 computer located in the control room. LabVIEW programs written specifically for this experiment were used for the data acquisition.

Video Signals

The unfiltered video signals traveled from the two eye cameras to the control room through the slip ring assembly above the CAP. From there, we attached a Y-connector to the cables so that the signals could run simultaneously to both the data acquisition computer and to a video data system (H.E. Inc. [HEI]) module. The HEI module added a bar code containing a time stamp and data from the analog signals (see below) to the video image. Using a pair of Hi-8 video cassette recorders, we recorded on videotape the appended video image, as well as all audio signals from the control room and from the CORO. The ISCAN system (refer to chapter 5) used the video signal fed directly into the computer to output four channels of digital eye position data stored on the computer's hard drive: horizontal eye position (left eye), vertical eye position (left eye), horizontal eye position (right eye), and vertical eye position (right eye). The ISCAN system also sent the video images to a pair of monitors, adding a cross hair centered over each pupil (see Figure 5.3 in chapter 5).

Analog Signals

In addition to the video signals, we collected 6 channels of analog data during each run as listed below:

1. *x*-axis accelerometer (A_x)
2. *y*-axis accelerometer (A_y)
3. *z*-axis accelerometer (A_z)
4. CAP command signal
5. CAP tachometer signal
6. Push-button signal

The push-button and accelerometer signals originated from their respective instruments in the CORO and traveled through a patch panel mounted on the CAP and through the slip rings to the control room. The push-button signal was connected to a small light bulb near the data acquisition computer. The accelerometer and tachometer signals traveled through a 50 Hz low-pass filter before arriving at the computer. The command signal fed directly into the data acquisition computer from the Wavetek in the control room. The attenuated tachometer signal is hard-wired directly into the control room. A flow chart illustrating the data connections is depicted in Figure 7.6.

LabVIEW Data Acquisition Program

The analog and ISCAN data was collected by the computer at a rate of 60 Hz, and were displayed and stored in binary format using a LabVIEW program. The program is written to collect both calibration and run data. For the calibration procedure, we input the interpupillary distance and the distance from the eye to the screen and the program collects the eye

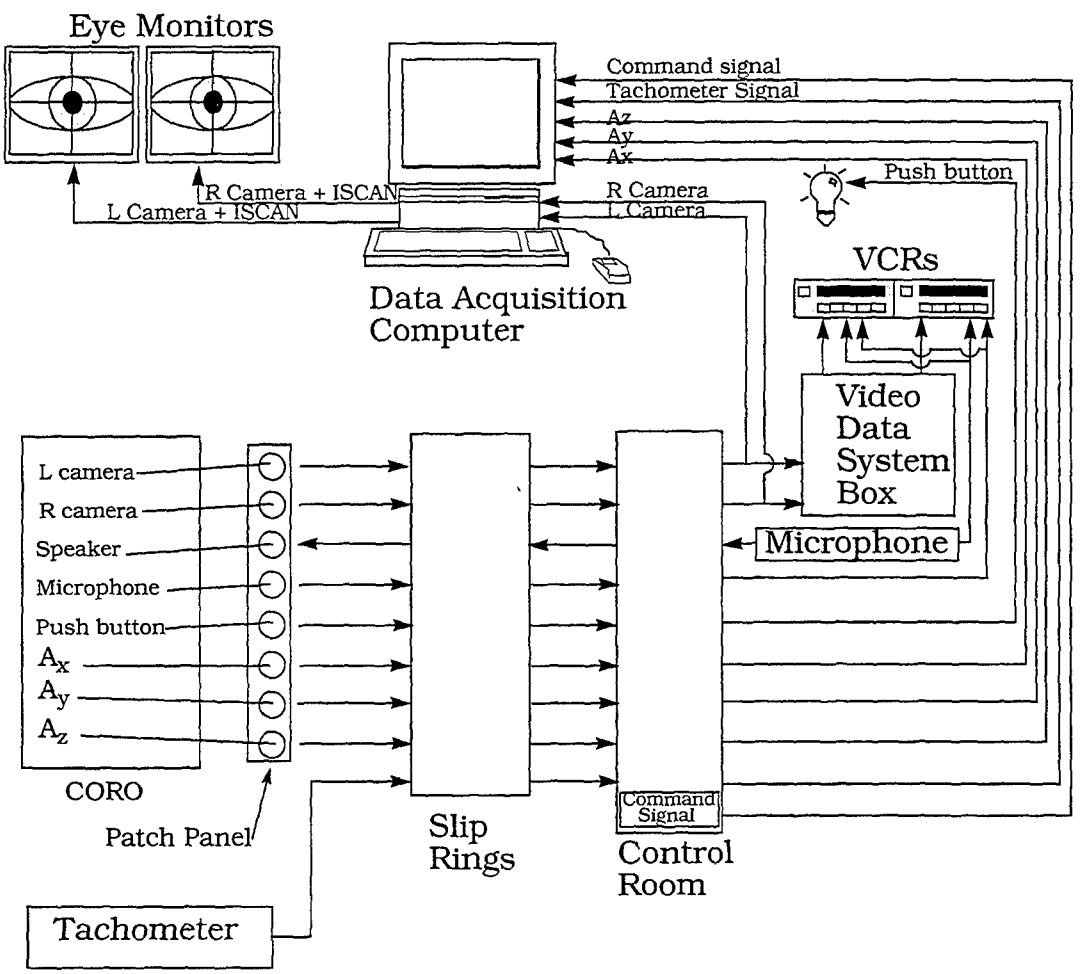

FIGURE 7.6. Flow of data

position data as the subject looks at each calibration LED. The program stores the calibration run data in a calibration file, then calculates and saves the calibration constants for each eye (see Appendix B). During the run, the program collects the eye position data and the filtered analog data and then stores the data to another file on the hard drive of the computer.

7.2.7 Analysis

Another LabVIEW program was written to convert the position of the pupil on the screen into the angular position of the eye using the eye calibration constants (see Appendix B) saved to the calibration file. This program also calculates the location of the subject's vergence point (x_{VP}, y_{VP}, and z_{VP} - see chapter 6) using the angular eye positions. The analysis program then outputs a new file containing 12 data columns: A_x, A_y, A_z, (the linear acceleration of CORO), θ_l, θ_r, ϕ_l, ϕ_r (the angular positions of the left and right eyes), x_{VP}, y_{VP}, z_{VP} (the location of the vergence point with respect to the head), and tachometer (which provides the angular velocity of the CAP).

To determine the angular velocity of the eyes, we used a commercial analysis program called Oculo1 v2.5.1a. This program contains algorithms specially written to filter and differentiate eye position data. Oculo1 applies an Order-Statistic filter on the raw eye position data and then numerically differentiates it. The resulting eye velocity data is then desaccaded and filtered again. (For more detail, refer to Engelken & Stevens, 1990.) The final product is the slow phase velocity of the eye. In Figure 7.7, we present a sample of eye position data as it looks after each step of the eye velocity analysis.

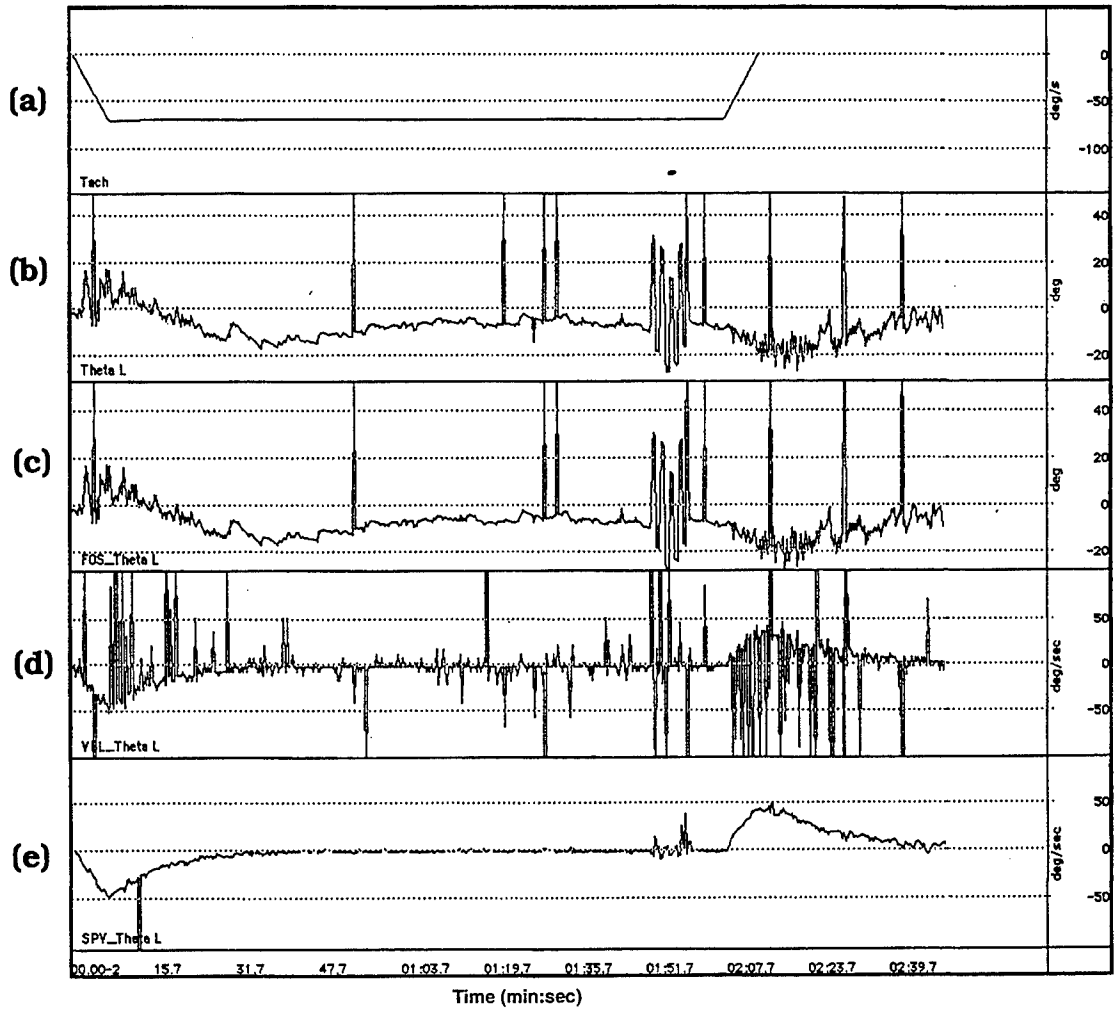

FIGURE 7.7. Sample results of eye velocity analysis. (a) The angular velocity stimulus (in deg/s) data is provided by the tachometer. (b) The horizontal angular position of the eye in degrees is recorded during the experiment. The spikes in the data occur when the subject blinks. (c) The angular eye position data filtered by Oculo 1. (d) The program then differentiates the filtered angular position data to obtain angular velocity of the eye in deg/s. Notice the spikes that result from differentiating the fast phase component of the eye position. (e) The spikes are removed by Oculo1, and the resulting slow phase velocity of the eye is the final product.

CHAPTER 8

EXPERIMENTAL RESULTS

8.1 Data

8.1.1 Eye velocity

For each run, we calculated velocity from the eye position data following the data analysis procedure described in section 7.2.7. From each velocity trace, we noted the peak eye velocity during acceleration of the subject. A summary of the peak velocity data for the forward-facing and backward-facing (tangential) 2g runs are listed in Table 8.1. When the CAP rotated in a counterclockwise direction, subjects 1 - 6 were forward-facing and subjects 7 - 14 were backward-facing. When the CAP rotated in a clockwise direction subjects 1 - 6 were backward-facing and subjects 7 - 14 were forward-facing.

TABLE 8.1. Peak Eye Velocity Data for 2g Runs (in deg/s)

Subject #	Forward Facing (CCW)	Backward Facing (CW)	Subject #	Forward Facing (CW)	Backward Facing (CCW)
1	-36	19	7	61	-28
2	-38	39	8	75	-41
3	-57	23	10	79	-52
4	-59	37	11	49	-21
5	-64	43	12	53	-28
6	-55	20	14	121	-14
AVERAGE	-52	30	AVERAGE	73	-31

If we ignore the direction of rotation and average together all the forward-facing run data and all the backward-facing run data, the average peak velocities are (disregarding signs):

Peak eye velocity (forward-facing) = 62 deg/s
Peak eye velocity (backward-facing) = 30 deg/s

Similarly, the eye velocity data from the 1g runs are listed in Table 8.2 below. During counterclockwise rotation, subjects 15 - 19 and 27 - 28 were forward-facing and subjects 21 - 26 were backward-facing. During clockwise rotation, subjects 15 - 19 and 27 - 28 were backward-facing and subjects 21-26 were forward-facing.

TABLE 8.2. Peak Eye Velocity for 1g Runs (in deg/s)

Subject #	Forward Facing (CCW)	Backward Facing (CW)	Subject #	Forward Facing (CW)	Backward Facing (CCW)
21	-31	36	15	46	-21
22	-36	15	16	54	-18
23	-51	40	17	22	-15
24	-38	46	19	36	-30
25	-20	26	27	52	-21
26	-33	20	28	18	-21
AVERAGE	-35	31	**AVERAGE**	38	-21

Again, if we ignore the direction of rotation and average together all the forward facing run data and all the backward facing run data, the averages are (disregarding signs):

Peak eye velocity (forward-facing) = 36 deg/s
Peak eye velocity (backward-facing) = 26 deg/s

8.1.2 Vergence

From the eye position data, we also constructed traces for the coordinates x_{VP}, y_{VP}, and z_{VP} that locate the vergence point, using the procedure described in chapter 6. The vergence data are more difficult to quantify because of the inconsistent results across subjects. For simplicity, we will concentrate only on x_{VP}, because the model presented in chapter 4 depends primarily on that variable.

The vergence point for each subject typically shifted gradually from one distance to another from the beginning to the end of the angular acceleration (see Figure 8.1 for a sample plot of x_{VP}).

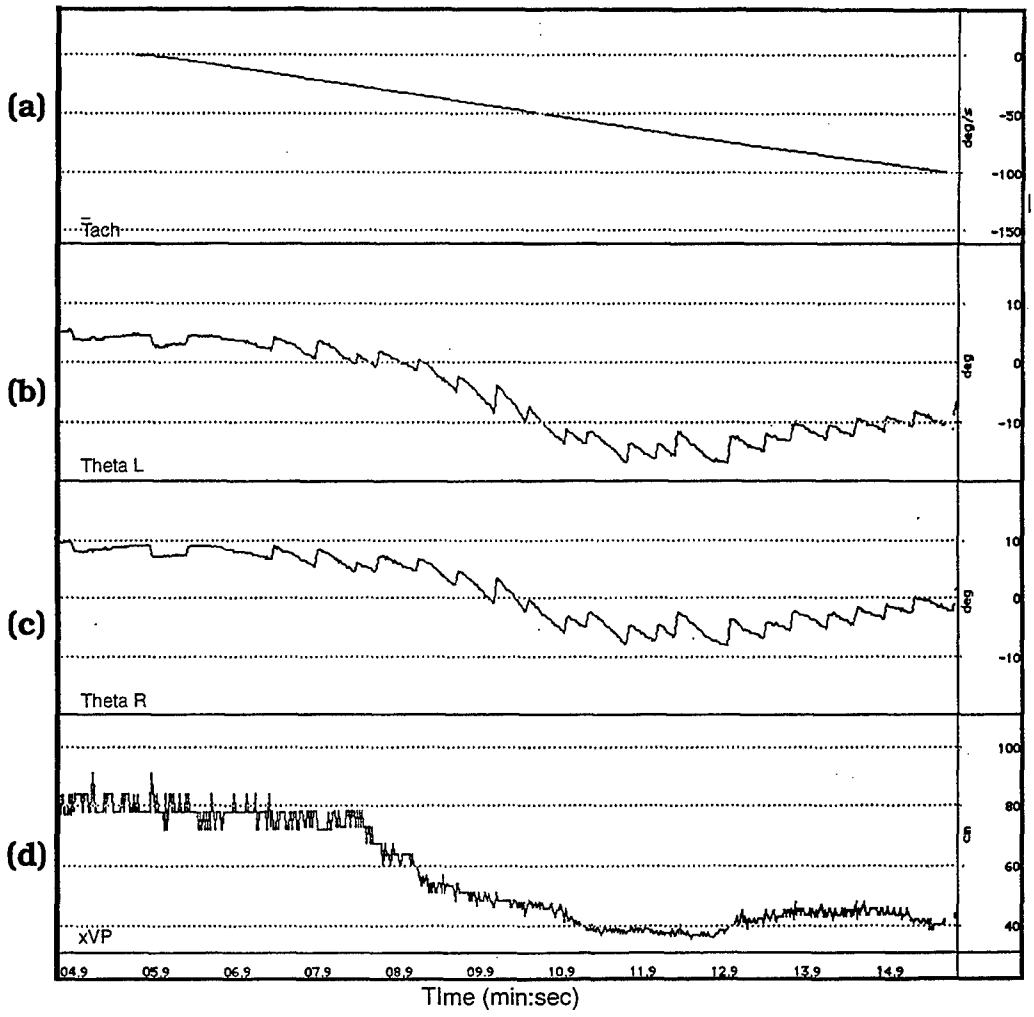

FIGURE 8.1. Sample vergence distance plot. (a) Tachometer signal (deg/s), (b) left eye position (deg), (c) right eye position (deg), and (d) vergence distance in the *x*-direction, x_{VP} (cm). Notice in (d) the drift in gaze distance towards the subject during acceleration.

The vergence point data for the 2g and 1g runs are presented in Tables 8.3 and 8.4, respectively. The values listed in the tables represent the

range of the vergence point distance (x_{VP}) for each subject during the acceleration portion of each run. The average values for each condition are also presented at the bottom of Tables 8.3 and 8.4; these values were obtained by averaging the mid-range values x_{VP} for each subject.

TABLE 8.3. Vergence Point Distance x_{VP} in cm (2g runs)

Subject #	Forward Facing (CCW)	Backward Facing (CW)	Subject #	Forward Facing (CW)	Backward Facing (CCW)
1	125-43	107-50	7	110-50	85-48
2	51-64	72-67	8	150-250	170-81
3	75-40	65-53	10	100-50	73-140
4	61-41	59-38	11	105-56	81-48
5	74-250	57-250	12	49-150	50-72
6	250-67	250-70	14	110-76	200-80
AVERAGE	95	85	AVERAGE	105	94

TABLE 8.4. Vergence Point Distance x_{VP} in cm (1g runs)

Subject #	Forward Facing (CCW)	Backward Facing (CW)	Subject #	Forward Facing (CW)	Backward Facing (CCW)
21	79-58	105-215	15	72-58	78-46
22	58-55	110-42	16	15-34	17-19
23	89-135	100-72	17	64-96	100-93
24	185-44	240-40	19	49-125	82-110
25	103-195	72-140	27	100-80	83-100
26	79-56	68-46	28	73-59	73-58
AVERAGE	112	104	AVERAGE	69	72

If we ignore the direction of rotation and average together all the forward-facing run data and all the backward-facing run data, the average vergence point distances for the 2g runs are:

average x_{VP} (forward-facing) = 100 cm
average x_{VP} (backward-facing) = 90 cm

We do the same for the 1g runs and find that the average vergence point distances are:

average x_{VP} (forward-facing) = 91 cm
average x_{VP} (backward-facing) = 88 cm

8.2 Discussion

8.2.1 Eye velocity

We do not wish to elaborate on the eye velocity data. We merely want to point out that we found the peak eye velocity data collected during acceleration followed the same trend as did those of the Lansburg et al. experiment. Specifically, the magnitude of the average peak eye velocity during the forward-facing runs was greater than that of the backward-facing runs.

8.2.2 Vergence

What is most surprising about the vergence data is their randomness. The only apparent similarity among the vergence distance plots is that the

vergence distance drifts during the acceleration portion of the runs. At the beginning of the run, the subject looks at a particular point and his gaze tends to drift either towards or away from him as he is angularly accelerated. Whether a subject's vergence point distance increased or decreased during acceleration appears to be random; there is no correlation between gaze distance and the subject's direction of motion.

The actual vergence distances tend to be random as well. The average values for x_{VP} during the forward-facing and backward-facing runs were not significantly different; neither were those for the 1g and 2g runs. Furthermore, the average vergence distance of about 1 m was much smaller than the 6 m we expected.

Most important, the gaze drift (regardless of whether it increased or decreased) is not at all consistent with the type of response expected if we suppose that vergence is the factor driving eye velocity in the dark. For a subject in the forward-facing condition following a visual "target" in the dark (as described in chapter 4), for example, we would expect an alternating pattern of decreasing x_{VP} during the slow phase portion of eye velocity followed by a return to its original value during the fast-phase portion of eye velocity. Instead, the vergence data more closely resembles what we might see in a subject who is fixating on a head-fixed (as opposed to an earth-fixed) target while rotating; subjects of such experiments exhibit suppressed VOR (Skipper & Barnes, 1989).

8.2.3 Possible sources of error

We encountered a few problems during the experiment which may have contributed to error in the data. First, despite our efforts to keep the sub-

ject's head still, we still found that some subjects shifted within the helmet. Although our head restraint system is capable of adequately immobilizing the head, it caused discomfort in most subjects. Not wanting our subjects in pain, we loosened the helmet if they were uncomfortable which led to head shift during acceleration. The head shift seemed primarily to be in the vertical direction, so it did not adversely affect our ability to measure eye position and hence calculate the eye velocity and position of the vergence point in the horizontal plane. The vertical component of eye position was affected, however. As a result, we could not locate the vertical position of the vergence point.

Second, a few of the subjects reported seeing a green glow in front of their eyes during the course of the experiment. We suspect these individuals were able to see the infra-red reflection from the mirrors of the illuminating LED. Such visual cues can alter the eye response; as mentioned earlier, the magnitude of eye movement changes with target distance.

Lastly, we did not check subjects for possible phoria abnormalities. When a phoric person looks at an object, then covers one eye, the covered eye tends to drift either left or right. Whether such a condition affects the ability of the eyes to converge in the dark is unknown.

CHAPTER 9

CONCLUSIONS

9.1 Determining Vergence

The CAP experiment proved that we are capable of determining the vergence point using the binocular eye-tracking system while rotating a subject in the dark. The limiting factors are how accurately the pupil is tracked and how well the head is restrained within the helmet. We must keep in mind, however, that even with a very reliable system, the vergence calculations are accurate to within 10% only when a person is looking at a point less than 1.5 m away. The accuracy decreases significantly when the vergence distance is between 1.5 and 3m, and beyond 3m it is virtually impossible to determine where a person is looking.

9.2 Vergence and VOR in the Dark

Based on the vergence data presented in chapter 8, we consider it reasonable to conclude that vergence is not the primary factor driving the VOR in the dark. Hence, the proposed model presented in chapter 4 does not correctly predict the VOR in the dark (although it may still be applicable

for predicting VOR when a subject gazes upon a visible target). The average vergence distance (92 cm) is significantly less than the distance predicted by the model. Furthermore, the vergence distance plots are not qualitatively consistent with what we would expect if the subjects were gazing on an imaginary target in the dark. The plots show instead that the gaze distance drifts, either increasing or decreasing gradually during acceleration. This type of response is more characteristic of what happens when a person gazes on a head-fixed target.

The difference in eye response during forward- and backward-facing runs might be otherwise explained. Merfeld (1990) and Sargent and Paige (1991) contend that the AVOR and LVOR are additive. In the forward-facing condition, the LVOR response to the centripetal acceleration acts in the same direction as does the AVOR response to the rotational stimulus; their sum is large. In the backward-facing condition, the LVOR opposes AVOR in direction and hence their sum is less than in the forward-facing condition.

The question remains: what drives the VOR in the dark? Collewijn (1989) suggests that there is no single factor. In any situation, the eyes continuously receive a variety of sensory inputs from all over the body: visual, vestibular, somatosensory (from the muscles), etc. These cues all contribute toward the eye motion response. In normal day-to-day operation, the eyes work well to compensate for the motion of the body. The VOR functions smoothly to stabilize retinal images because the eyes are receiving all the information they need to respond accurately. When a person rotates (or is subjected to any other type of motion, for that matter) in the dark, the eyes no longer receive the visual information. The VOR can no longer function correctly in the dark because an important piece of infor-

mation is missing. That the eyes respond to motion in the dark is no longer a mystery when we consider Collewijn's view. Even though the eyes are deprived of visual stimuli, the other senses function unimpaired; the vestibular and somatosensory continue to communicate with the eyes, which respond, albeit inadequately.

REFERENCES

Benson, A. J. (1982). The vestibular sensory system. In H. B. Barlow & J. D. Mollon (Eds.), *The Senses,* (pp. 333-68). Cambridge, England: Cambridge University Press.

Boff, K. R., & Lincoln, J. E. (1988). *Engineering Data Compendium: Human Perception and Performance.* Wright-Patterson AFB, OH: AAMRL.

Collewijn, H. (1989). The vestibulo-ocular reflex: An outdated concept? *Progress in Brain Research, 80,* 197-209.

Einstein, A. (1945). *The meaning of relativity.* Princeton, NJ: Princeton University Press.

Engelken, E. J., & Stevens, K. W. (1990). A new approach to the analysis of nystagmus: An application for order-statistic filters [Technical Note]. *Aviation, Space, and Environmental Medicine, 61,* 859-64.

Gillingham, K. K., & Wolfe, J. W. (1986). *Spatial orientation in flight.* (USAF Technical Report USAFSAM-TR-85-31). Brooks Air Force Base, TX: USAF School of Aerospace Medicine.

Hardy, M. (1934). Observations on the innervation of the macula sacculi in man. *Anatomical Record, 59,* 403-78.

Hixson, W. C., & Anderson, J. J. (1966). *The Coriolis acceleration platform: A unique vestibular research device.* (NASA Report R-93). Pensacola, FL: Naval Aerospace Medical Institute.

ISCAN, Inc. (1994). *RK-426PC Pupil/corneal reflection tracking system (PC card version) operating instructions.* Cambridge, MA: Author.

Lansberg, M. P., Guedry, F. E., Jr., & Graybiel, A. (1965). The effect of changing the resultant linear acceleration relative to the subject on nystagmus generated by angular acceleration. *Aerospace Medicine, 36,* 456-60.

McGrath, B. J. (1990). *Human vestibular response during 3 G_z centrifuge stimulation.* Master's thesis, Massachusetts Institute of Technology, Cambridge.

McGrath, B. J., Guedry, F. E., Oman, C. M., & Rupert, A. H. (1995). Vestibulo-ocular response of human subjects seated in a pivoting support system during 3 G_z centrifuge stimulation. *Journal of Vestibular Research, 5,* 331-47.

Merfeld, D. M. (1990). *Spatial orientation in the squirrel monkey: An experimental and theoretical investigation.* Doctoral dissertation, Massachussetts Institute of Technology, Cambridge.

Moore, S. T., Haslwanter, T., Curthoys, I. S., & Smith, S. T. (1996). A geometric basis for measurement of three dimensional eye position using image processing. *Vision Research, 36,* 445-59.

Naval Aerospace Medical Institute (1991). *Environmental physiology operational medicine text.* Department of the Navy.

Paige, G. D. (1989). The influence of target distance on eye movement responses during vertical linear motion. *Experimental Brain Research, 77,* 585-593.

Paige, G. D. (1991) Linear vestibulo-ocular reflex (LVOR) and modulation by vergence. *Acta Otolaryngologica (Stockholm),* (Suppl. 481), 282-286.

Paige, G. D., & Tomko, D. L. (1991). Eye movement responses to linear head motion in the squirrel monkey. II. Visual-vestibular interactions and kinematic considerations. *Journal of Neurophysiology, 65,* 1183-96.

Robinson, D. A. (1981). Control of eye movements. In V. B. Brooks (Ed.), *Handbook of physiology: Vol. II, Part 2 - The nervous system* . (pp.1275-1320). Washington, DC: American Physiological Society.

Sargent, E. W., & Paige, G. D. (1991). The primate vestibulo-ocular reflex during combined linear and angular head motion. *Experimental Brain Research, 87,* 75-84.

Skipper, J. J., & Barnes, G. R. (1989). Eye movements induced by linear acceleration are modified by visualisation of imaginary targets. *Acta Otolaryngologica (Stockholm),* (Suppl. 468), 289-293.

Viirre E., Tweed, D., Milner, K., & Vilis, T. (1986). A reexamination of the gain of the vestibuloocular reflex. *Journal of Neurophysiology, 56,* 439-50.

Wearne, S. (1993). *Spatial orientation of the human linear and angular vestibulo-ocular reflexes during centrifugation.* Doctoral dissertation, University of Sydney, Sydney, Australia.

Wilson, J. W., & Jones, G. M. (1979). *Mammalian vestibular physiology.* New York: Plenum Press.

Young, L. R., & Sheena, D. (1975). Methods and designs: Survey of eye movement recording methods. *Behavior and Research Methods and Instrumentation, 7,* 397-429.

APPENDIX A

VOR PROGRAM CODE (MATLAB)

```
%program vor
%this program calculates the angular displacement
%and velocity response due to LVOR and AVOR when a person is
%rotated about an axis at distance R with a constant angular
%acceleration. The person is assumed to have his gaze fixed
%on a point that is initially straight ahead at a distance D
%the subject is facing towards (backward facing) or away
%from (backward facing) the direction of rotation

% PARAMETERS
R=20;       %(ft) radius of centrifuge
D=20;  %(ft) distance of gaze
alpha=10.0*pi/180;    %(deg/s^2 converted to rad/s^2)  angular accel. of
CAP
reset=-20*pi/180;     %(deg converted to rad) max angular excursion of
the eye
tsacc=0.075;  %time required to complete saccade
dt=0.001;
nsacc=tsacc/dt;       %number of time increments to complete saccade

% EQUATIONS OF MOTION:
t=0:dt:8.4;
w=alpha*t;                          %(rad/s)  angular vel. of CAP
phi=0.5*alpha*t.*t;                   %(rad) angular disp. of CAP

% EYES
%     EYE POSITION
th=zeros(1,length(t));                %initializes th vector
phir=0;   %initializes phi reset
for i=1:length(t);
  yl=R-cos(phi(i)-phir).*R;
%  xl=D-sin(phi(i)-phir).*R;            %forward facing
```

```
  xl=D+sin(phi(i)-phir).*R;          %backward facing
  thl=atan2(yl,xl);                  %(rad) ang disp due to LVOR
 th(i)=-phi(i)+phir-thl; %(rad) ang disp of the eye(AVOR+LVOR)
  if th(i)<=reset;
  if (i+nsacc)<length(t);phir=phi(i+nsacc);end
th(i)=reset;
  end
end

%add saccade to position profile
for i=2:length(t)
  if th(i)==reset;
if (i+nsacc)<length(t);
for j=i+1:i+nsacc-1;th(j)=th(j-1)+(0-reset)/tsacc*dt;end
end
  end
end

%EYE VELOCITY
weye=diff(th)./dt;                %(rad/s) angular velocity of the eye

%   fix angular velocity during saccade (make it linear)
sumw=0;
sumt=dt;
for i=2:length(t)-1;
   if th(i)==reset;
   if (i+nsacc)<=length(t);
  slope=(weye(i+nsacc)-weye(i-2))/(tsacc+2*dt);
wmax=weye(i+nsacc);
tmax=t(i+nsacc);
wmin=weye(i-2);
tmin=t(i-2);
for j=i-1:i+nsacc-1;
weye(j)=weye(j-1)+slope*dt;
sumw=sumw+weye(j);
sumt=sumt+t(j);
end
end

if (i+nsacc)>length(t);
for j=i-1:length(t)-1;weye(j)=weye(j-1)+slope*dt;end
```

```
      end
   end
end

%AVERAGE, MAX, MIN EYE VELOCITY

savg=sumw/sumt*180/pi;
smax=wmax/tmax*180/pi;
smin=wmin/tmin*180/pi;
wavg=zeros(1,2);
wmin=zeros(1,2);
wmax=zeros(1,2);
t2=zeros(1,2);

wavg(2)=savg*length(t)*dt;
wmin(2)=smin*length(t)*dt;
wmax(2)=smax*length(t)*dt;
t2(2)=length(t)*dt;


t1=dt:dt:8.4;
th=th*180/pi;
weye=weye*180/pi;
axis([1 2 3 4]);axis;
axis('normal')
%plot(t,th,t1,weye,'--',t2,wavg,'-.',t2,wmin,':',t2,wmax,':')
plot(t,th,'w',t1,weye,'w--',t2,wavg,'w-.')
%title('Angular Displacement and Velocity of the Eye (Forward Facing)')
title('Angular Displacement and Velocity of the Eye (Backward Facing)')
xlabel('Time (s)')
ylabel('Displacement (deg), and Velocity (deg/s)')
%text(3,-110,'alpha=10 deg/s^2, reset=-20 deg')
text(1,-75,'___ Angular displacement')
text(1,-85,'- - - Angular velocity')
text(1,-95,'-.-.- Average angular velocity')
grid
```

APPENDIX B

ISCAN CALIBRATION

B.1 Introduction

The ISCAN system tracks the center of the pupil and reports its location in terms of pixels on a video screen. Because we are interested in the angle through which the eye travels, we must employ a calibration algorithm that converts the pixel output to angle data for each eye. To derive the calibration calculations, we must make the following assumptions (Moore, et al., 1996):

1. The eye is a perfect sphere and rotates about the center of this sphere.
2. The eye exhibits ideal "ball and socket" behavior, so that all eye movements are pure rotations around the center of the eye, with no translation of this center.
3. The camera is directly in front of the eye, and the image of the eye corresponds to a parallel projection of the eye into the image plane.

B.2 Calibration

We monitor the subject's eyes using a pair of COHU high resolution infrared cameras. For each eye, the ISCAN system tracks the center of the pupil on the screen and superimposes a crosshair onto the eye display.

ISCAN divides the square monitor screen horizontally into 512 pixels, and vertically into 256 pixels, then reports the pixel position (P_y,P_z) of the pupil center. Pixel (0,0) is located in the upper left-hand corner, and pixel (511, 255) is located in the lower right-hand corner. In order to simplify future calculations, we superimpose a cartesian *YZ*-coordinate system to locate the center point of each pixel; the origin of the new coordinate system is located at the center of the video screen, and both *Y* (the horizontal coordinate) and *Z* (the vertical coordinate) vary from -256 to 256. We use the following equations to convert the (P_y,P_z) pixel position into the more practical (*Y*,*Z*) coordinates:

$$Y = \frac{2P_y + 1}{2} - 256 \qquad \text{(EQ B.1)}$$

$$Z = 256 - (2P_z + 1) \qquad \text{(EQ B.2)}$$

The pixel coordinate system and the transformed screen coordinate system are illustrated in Figure B.1.

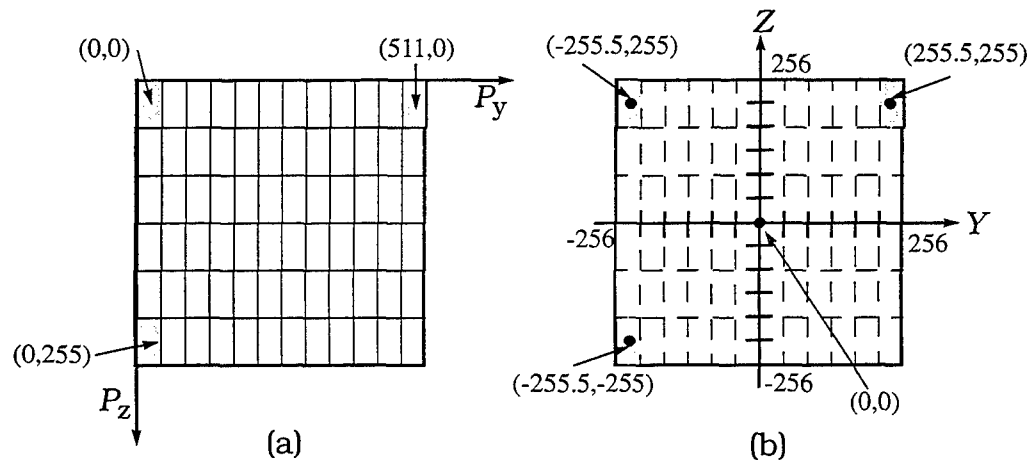

FIGURE B.1. Screen Coordinates. (a) Pixel coordinate system (P_y,P_z), and (b) transformed screen coordinate system (*Y*,*Z*).

Because we are interested in the angular position of the eye, we now require a set of calibration equations to convert the transformed screen coordinates (Y,Z) into the angles θ and ϕ. After collecting some initial data we found that θ and ϕ are best described by the following pair of linear equations:

$$\theta = C_h Y + b_h \quad \text{(EQ B.3)}$$

$$\phi = C_v Z + b_v \quad \text{(EQ B.4)}$$

We describe how to calculate the constants C_h, C_v, b_h, and b_v from data acquired during the calibration procedure in Section B.2.2.

B.2.1 Calibration procedure

Each subject must undergo the calibration procedure each time the cameras are adjusted. For this experiment we use a calibration "cross" of lights that are embedded in the device's curved screen. The cross consists of five equally spaced LEDs arranged along a curved line in the horizontal plane, and five equally spaced LEDs arranged in a vertical line. The two lines of LEDs share the center LED (see Figure B.2). The horizontal LEDs are numbered 1 through 5, left to right, and the vertical LEDs are numbered 6 through 9, top to bottom (skipping the middle LED). The subject is positioned such that the center of the cross is aligned with a point on the subject's face midway between the eyes.

Using a digital pupillometer, we measure the subject's interpupillary distance before we position him or her in the device. We also require the distance d from the center of the subject's eye to the center of the calibration

cross (see Figure B.3). After the subject is in place and the eye cameras have been adjusted, we use a ruler to measure from the corner of the eye (approximating it as the center of the eye) to the plate behind the head to which the helmet is fixed. We know from a previous measurement the distance from the plate to the center of the screen. To find *d*, we subtract the head plate-to-eye distance from the plate-to-screen distance. We then instruct the subject to look at each point of the calibration cross in turn as we collect the pupil position data. We perform the calibration twice and use the averaged data for the calculations that follow.

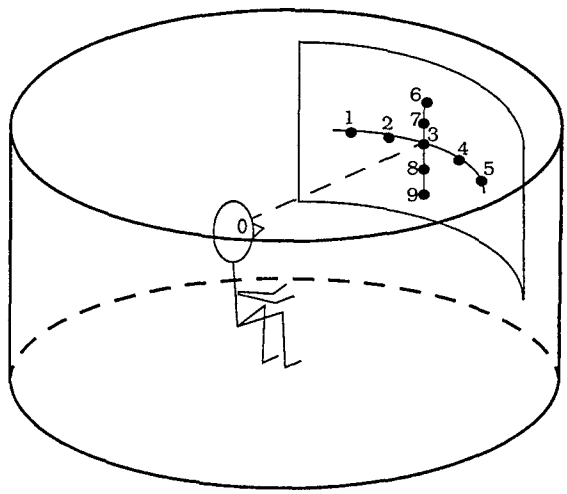

FIGURE B.2. Calibration Cross

Horizontal Calibration

The horizontal calibration configuration is illustrated in Figure B.3 (the dots numbered 1 - 5 represent the horizontally arranged LEDs). Note that

although only the right eye is depicted, we perform the calibration and record pupil position data for both eyes simultaneously.

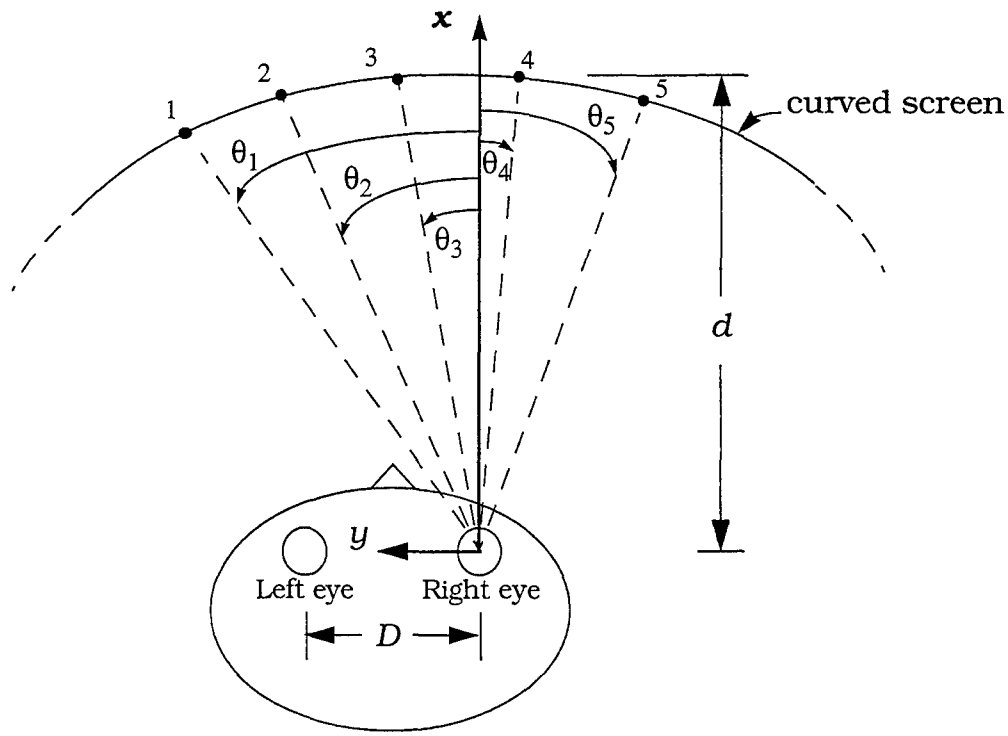

FIGURE B.3. Horizontal calibration configuration (looking down on subject).

In order to calculate the calibration factors C_h and b_h, we must know the value of each θ_i, the horizontal angle through which the eye travels from the reference position to look at LED i (i = 1 - 5). We calculate θ_i for each eye based on the geometry:

$$\theta_i = \text{atan}\left(\frac{y_i}{x_i}\right) \qquad \text{(EQ B.5)}$$

The variables y_i and x_i, distances that locate the LED i from the center of the eye, are illustrated in Figure B.4. Note from Figures B.3 and B.4 that

in accordance with the right-handed coordinate system, y_i and θ_i are both positive when the subject looks leftward. We calculate y_i and x_i in terms of the measured distances D and d, and the geometric distances h_i and a_{ij} (i and j vary from 1 - 5), which are depicted in Figure B.4. The variables y_i and x_i are mathematically defined in Table B.1.

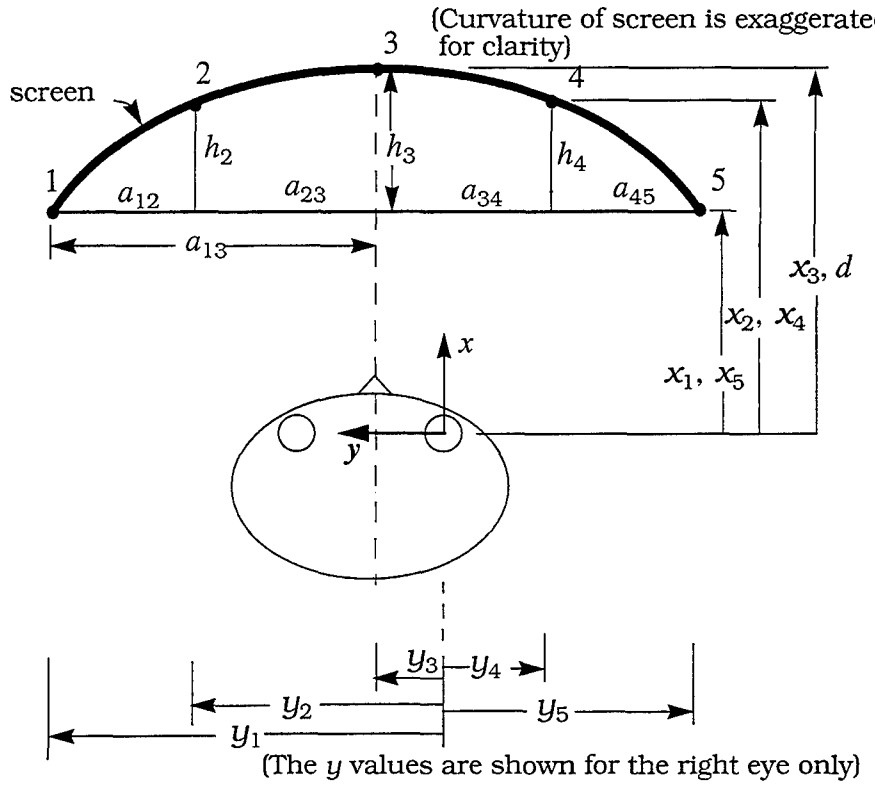

Note: a_{ij} represents the perpendicular distance between LEDs i and j

$a_{13} = a_{12} + a_{23}$
$a_{34} = a_{23}$ and $a_{45} = a_{12}$
$x_1 = x_5$ and $x_2 = x_4$
$x_3 = d$
$h_2 = h_4$

FIGURE B.4. Geometry of horizontal calibration setup (looking down on subject)

TABLE B.1. y_i and x_i for Both Eyes

LED #	y_i Left eye	y_i Right Eye	x_i Both eyes
1	$a_{13} - D/2$	$a_{13} + D/2$	$d-h_3$
2	$a_{23} - D/2$	$a_{23} + D/2$	x_1+h_2
3	$-D/2$	$D/2$	d
4	$-(a_{23} + D/2)$	$-(a_{23} - D/2)$	x_1+h_2
5	$-(a_{13} + D/2)$	$-(a_{13} - D/2)$	$d-h_3$

We further describe the distances h_i and a_{ij} in terms of the measured radius of the screen R, and θ_{ij}, the angle formed across the arc between LEDs i and j, as illustrated in Figure B.5.

$$a_{ij} = R(\sin\theta_{ij}) \qquad \text{(EQ B.6)}$$

The angle θ_{ij} is geometrically defined in terms of R and the measured arc-length A_{ij} between LEDs i and j, which are also illustrated in Figure B.5.

$$\theta_{ij} = \frac{A_{ij}}{R} \qquad \text{(EQ B.7)}$$

Note from Tables B.1 and B.2 that we need Equations B.6 and B.7 only to calculate θ_{13}, θ_{23}, a_{13} and a_{23}.

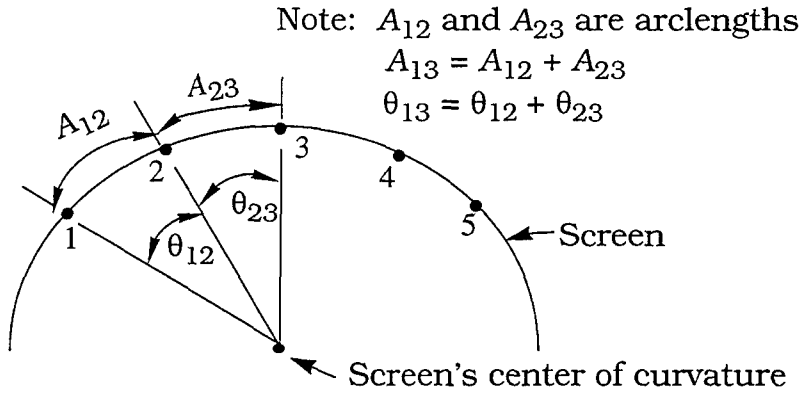

FIGURE B.5. Geometry of the horizontal LEDs on the curved screen

Vertical Calibration

The vertical calibration is similar to the horizontal calibration. We instruct the subject to look at each LED from top to bottom (LED numbers 6, 7, 3, 8, 9) as we collect ISCAN data. We must determine the values of ϕ_i for each eye as the subject looks from one LED to the next. Based on the geometry (see Figure B.6), we define ϕ_i as follows:

$$\phi_i = \text{atan}\left(\frac{-z_i}{\sqrt{\left(\frac{D}{2}\right)^2 + d^2}}\right) \qquad \text{(EQ B.8)}$$

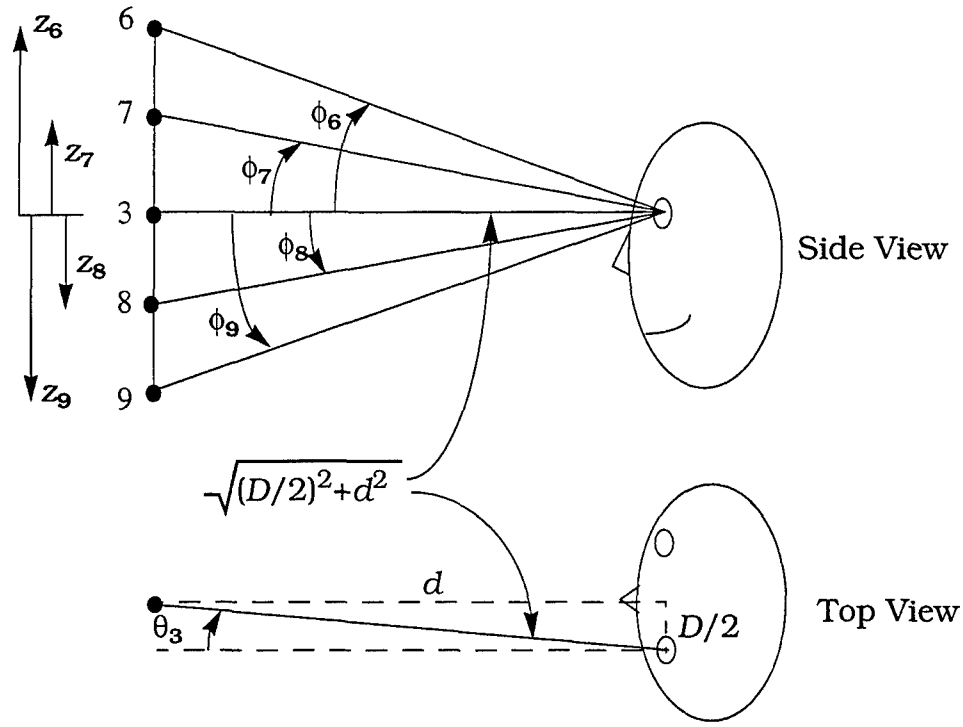

FIGURE B.6. Vertical Calibration configuration

where z_i represents the vertical distance of the LED i from the center LED. Note that when z_i is positive (i.e., LED i is located above the center LED) ϕ_i is negative, which is consistent with the right-handed coordinate system. Also notice that the horizontal angle θ that the eye makes to look at each of the vertical calibration LEDs is not zero, but is equal to θ_3, and that ϕ_i for the left eye equals ϕ_i for the right eye.

B.2.2 Calibration factors

The next step is to calculate the calibration factors C_v, C_h, b_v, and b_h, introduced in Equations B.3 and B.4. From the calibration procedure, we

know the values of Y_i and Z_i, the transformed pixel coordinates that describe the location of the center of the pupil on the screen for each calibration LED, and θ_i and ϕ_i, which we calculated from Equations B.5 and B.8, respectively. We perform a linear regression on θ_i vs. Y_i for $i = 1$ to 5, where Y_i is the independent variable. The slope of this line is C_h and the intercept is b_h. Similarly, with the vertical data we perform a linear regression on ϕ_i vs. Z_i for $i = 6, 7, 3, 8, 9$, where Z_i is the independent variable. The slope of this line is C_v and the intercept is b_v. We now possess all the information necessary to calibrate the experimental data.

B.3 Applying the Calibration Factors

Upon completing the calibration procedure, we have the following necessary values: C_v, C_h, b_v, and b_h. We can now convert a transformed pixel value (Y,Z) into the angular position of the center of the pupil (θ,ϕ). We enter the (Y,Z) coordinates into Equations B.3 and B.4, which we cite again here:

$$\theta = C_h Y + b_h \qquad \text{(EQ B.3)}$$

$$\phi = C_v Z + b_v \qquad \text{(EQ B.4)}$$

If we wish to describe the position of the pupil in terms of the head-fixed *xyz*-coordinates, we enter the values of θ and ϕ from Equations B.3 and B.4 into Equations 5.1, 5.2 and 5.3 (presented in chapter 5).

B.4 Verification of the Calibration Technique

We verified the integrity of the calibration procedure by running the calibration data for one subject through the analysis program. We compared the calculated angles θ and ϕ with the known angles required to look at each LED. The data, presented under Test 1 in Appendix C, confirms that the relationships between θ and Y, and between ϕ and Z, are indeed quite linear within the range of eye motion. We found that we can calculate the angle θ within 5% accuracy except when the angles are very close to zero (<3 degrees). The calculation of the vertical angle is slightly less accurate, probably due to a slight tilt about the y-axis in the position of the cameras with respect to the eyes. Nevertheless, we can calculate the angle ϕ within 6% accuracy over the range of eye motion.

APPENDIX C

VERIFICATION OF CALIBRATION AND VERGENCE ALGORITHM

Test 1

The results from Test 1 are presented below, as are the measured interpupillary distance D and the distance d from the subject's eye to the screen. We followed the calibration procedure as described in Appendix B to calculate the positional angles of the eyes, θ and ϕ, from the measured values of d and D. In Tables C.1 and C.2, we list the horizontal calibration data for the left and right eyes, respectively. The distances x_i and y_i that locate the position in the horizontal plane of LED i with respect to the eye were calculated based on the measured distances d and D. The horizontal coordinate of the pupil's center on the screen Y_i was obtained from ISCAN. The actual values of θ_i, the horizontal angular position of the eye, were calculated from x_i and y_i, and the calculated θ_i were determined by the analysis program.

The linearity of the horizontal calibration across the range of our measurements is apparent in the graphs shown in Figures C.1 and C.2, where we plot θ versus Y for the left and right eyes, respectively.

Subject Data: $D = 6.15$ cm
$d = 59.0$ cm

TABLE C.1. Left Eye Horizontal Calibration

LED#	x (cm)	y (cm)	Y	θ actual (rad)	θ calculated (rad)	% error
1	55.6	17.9	-31.5	0.311	0.312	0.4
2	58.2	7.5	2.5	0.129	0.124	3.8
3	59.0	-3.1	33.2	-0.052	-0.046	11.0
4	58.2	-13.7	67.0	-0.231	-0.233	1.06
5	58.6	-24.0	98.4	-0.408	-0.407	0.1

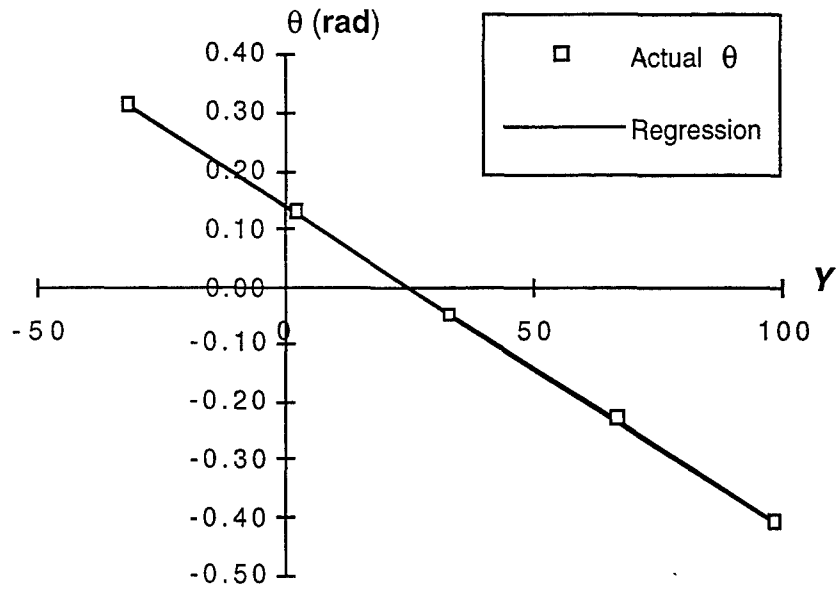

FIGURE C.1. θ versus Y for the left eye

TABLE C.2. Right Eye Horizontal Calibration

LED#	*x* (cm)	*y* (cm)	*Y*	θ actual (rad)	θ calculated (rad)	% error
1	55.6	24.0	-8.3	0.408	0.408	0.2
2	58.2	13.7	23.6	0.231	0.228	1.5
3	59.0	3.1	53.5	0.052	0.058	11.0
4	58.2	-7.5	87.0	-0.129	-0.133	3.1
5	55.6	-17.9	118.2	-0.311	-0.310	0.4

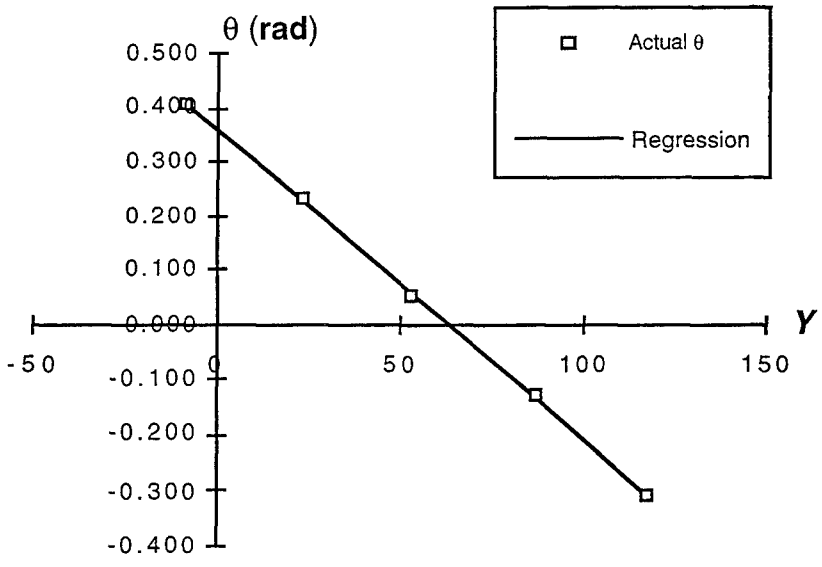

FIGURE C.2. θ versus *Y* for the right eye

In Tables C.3 and C.4, we present the vertical eye data for the left and right eyes, respectively. Listed are the x_i and z_i coordinates that locate the position of LED i with respect to the eye, the vertical coordinate of the pupil center on the screen Z_i, and the actual and calculated values of ϕ_i.

The x_i and z_i coordinates are calculated from the measured distances d and D. The actual ϕ_i are derived from D, x_i, z_i. The calculated ϕ_i were obtained from the analysis program. Again, the linearity of the calibration data for the vertical data is evident in the graphs shown in Figures C.3 and C.4, where ϕ versus Z is plotted for the left and right eyes, respectively.

TABLE C.3. Left Eye Vertical Calibration

LED#	x (cm)	z (cm)	Z	ϕ actual (rad)	ϕ calculated (rad)	% error
6	59.0	16.3	7.7	-0.270	-0.259	4.0
7	59.0	8.0	-16.8	-0.135	-0.143	5.7
3	59.0	0	-44.6	0.000	-0.011	-
8	59.0	-8.0	-76.4	0.135	0.140	3.4
9	59.0	-16.3	-104.6	0.270	0.273	1.3

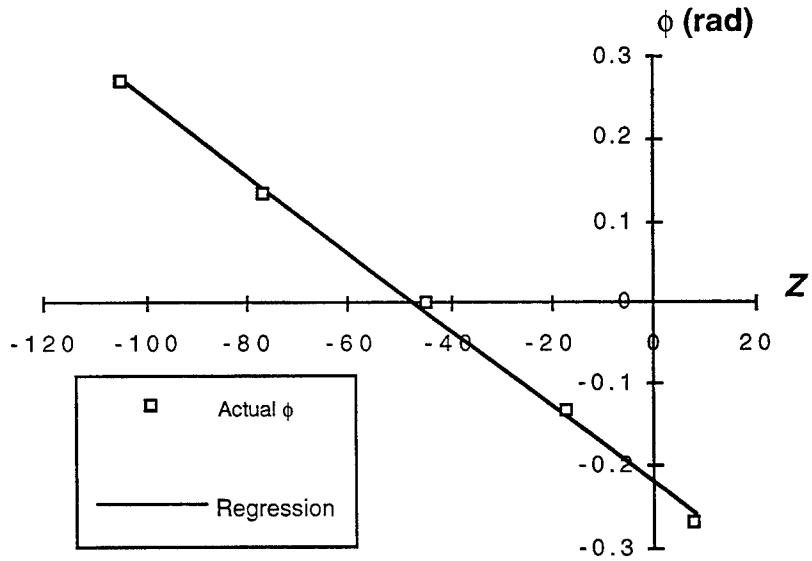

FIGURE C.3. ϕ versus Z for the left eye

TABLE C.4. Right Eye Vertical Calibration

LED#	*x* (cm)	*z* (cm)	*Z*	ϕ actual (rad)	ϕ calculated (rad)	% error
6	59.0	16.3	81.6	-0.270	-0.263	2.7
7	59.0	8.0	57.1	-0.135	-0.144	6.8
3	59.0	0	37.4	0.000	-0.001	-
8	59.0	-8.0	-1.1	0.135	0.137	1.2
9	59.0	-16.3	-28.9	0.270	0.271	0.4

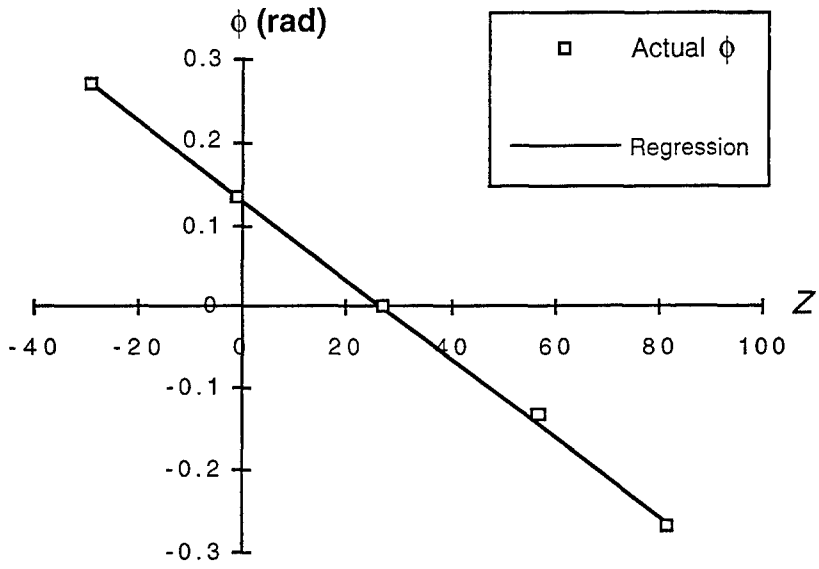

FIGURE C.4. ϕ versus *Z* for the right eye

The distances locating the vergence point (x_{VP}, y_{VP}, z_{VP}) calculated by the analysis program are listed below along with the actual distances locating the position of the LEDs (x,y,z).

TABLE C.5. Vergence Analysis of Calibration Data

LED #	x_{VP} (cm)	x (cm)	% Error	y_{VP} (cm)	y (cm)	% Error	z_{VP} (cm)	z (cm)	% Error
1	56.0	55.6	0.7	21.2	21.0	1.0	-1.8	0.0	-
2	57.5	58.2	1.3	10.2	10.6	3.6	-1.0	0.0	-
3	59.0	59.0	0.0	0.3	0.0	-	-1.2	0.0	-
4	59.0	58.2	1.4	-11.0	-10.6	3.3	-1.7	0.0	-
5	55.2	55.6	0.8	-20.8	-21.0	1.0	-3.1	0.0	-
6	62.1	59.0	5.3	0.7	0.0	-	16.6	16.3	1.6
7	62.7	59.0	6.2	0.6	0.0	-	9.1	8.0	13.0
3	61.3	59.0	3.9	0.4	0.0	-	0.4	0.0	-
8	59.3	59.0	0.5	0.4	0.0	-	-8.3	-8.0	2.9
9	61.0	59.0	3.3	0.4	0.0	-	-17.0	-16.3	4.2

Test 2

The calculated x_{VP} and the actual distances x of the points the subject looked at during Test 2 are listed below.

TABLE C.6. Calculated and Actual Vergence Distance: Test 2

x_{VP} (cm)	x (cm)	% Error
46.1	49	6.3
33.4	36	7.8
20.7	20	3.4
33.4	35	4.8
46.1	47	2.0

Test 3

The calculated x_{VP} and the actual distances x for the targets the subject looked at for Test 3 are listed below.

Subject data: D = 6.5 cm
d = 83.82 cm

TABLE C.7. Calculated and Actual Vergence Distance: Test 3

x_{VP} (cm)	x (cm)	% Error
65.0	61.0	6.6
74.0	76.2	2.9
90.0	91.4	1.5
110.0	106.7	3.1
125.0	121.9	2.5
140.0	137.1	2.1
140.0	152.4	8.1
160.0	182.9	12.5
140.0	213.4	34.4
160.0	243.8	34.4
170.0	274.3	38.0
200.0	304.8	34.4
200.0	335.3	40.4
250.0	365.8	31.7
200.0	396.2	49.5
310.0	426.7	27.4
310.0	457.2	32.2
310.0	487.7	36.4
518.2	310.0	67.2
548.6	310.0	77.0
579.1	420.0	37.9
609.6	420.0	45.1

APPENDIX D

LIST OF SUBJECT RUNS

The CORO position and direction of rotation for each subject's runs are listed in the tables below in the order that they were performed. Subject 13 was meant to duplicate subject 10's data, but because he asked to stop after the third run, we discarded subject 13's data. We decided to throw out the data from subject 9 because we had difficulty tracking his right eye; we ran subject 14 as a duplicate.

TABLE D.1. 2g Runs

Subj #	Run 1	Run 2	Run 3	Run 4	Run 5	Run 6
1	90 CW	90 CCW	110 CW	110 CCW	70 CW	70 CCW
2	70 CW	70 CCW	110 CW	110 CCW	90 CW	90 CCW
3	90 CCW	90 CW	70 CCW	70 CW	110 CCW	110 CW
4	110 CCW	110 CW	70 CCW	70 CW	90 CCW	90 CW
5	110 CW	110 CCW	90 CW	90 CCW	70 CW	70 CCW
6	70 CCW	70 CW	90 CCW	90 CW	110 CCW	110 CW
7	290 CCW	290 CW	270 CCW	270 CW	250 CCW	250 CW
8	250 CCW	250 CW	290 CCW	290 CW	270 CCW	270 CW
9	270 CCW	270 CW	250 CCW	250 CW	290 CCW	290 CW
10	290 CW	290 CCW	270 CW	270 CCW	250 CW	250 CCW
11	250 CW	250 CCW	290 CW	290 CCW	270 CW	270 CCW
12	270 CW	270 CCW	250 CW	250 CCW	290 CW	290 CCW
13	290 CW	290 CCW	270 CCW			
14	270 CCW	270 CW	250 CCW	250 CW	290 CCW	290 CW

We used subject 27's data to replace subject 20's data which we discarded because we couldn't track the left eye. Subject 28 replaces subject 18 who had droopy upper eyelids.

TABLE D.2. 1g Runs

Subj #	Run 1	Run 2	Run 3	Run 4	Run 5	Run 6
15	290 CCW	290 CW	270 CCW	270 CW	250 CCW	250CW
16	250 CCW	250 CW	290 CCW	290 CW	270 CCW	270 CW
17	270 CW	270 CCW	250 CW	250 CCW	290 CW	290 CCW
18	290 CW	290 CCW	270 CW	270 CCW	250 CW	250 CCW
19	250 CW	250 CCW	290 CW	290 CCW	270 CW	270 CCW
20	270 CCW	270 CW	250 CCW	250 CW	290 CCW	290 CW
21	110 CCW	110 CW	70 CCW	70 CW	90 CCW	90 CW
22	90 CW	90 CCW	110 CW	110 CCW	70 CW	70 CCW
23	70 CCW	70 CW	90 CCW	90 CW	110 CCW	110 CW
24	110 CW	110 CCW	70 CW	70 CCW	90 CW	90 CCW
25	90 CCW	90 CW	110 CCW	110 CW	70 CCW	70 CW
26	70 CW	70 CCW	110 CW	110 CCW	90 CW	90 CCW
27	270 CCW	270 CW	250 CCW	250 CW	290 CCW	290 CW
28	290 CW	290 CCW	270 CW	270 CCW	250 CW	250 CCW

APPENDIX E

SUBJECT BRIEF AND CONSENT FORM

15 Feb 1996

(If subject wears glasses, make sure he/she can see without them)

INSTRUCTIONS

1. Explain nature of experiment:
   - We are studying how your eyes respond when we subject you to a rotational stimulus.
   - You will be seated in a light proof cylindrical capsule that is located on the end of a rotating arm. (Show them model) We will rotate you at a constant velocity for approximately two minutes at (1 or 2) g. During this time, you will be completely in the dark and we will be videotaping your eye motions with infrared cameras. You will be asked to perform an audio task throughout the run. You will listen to a series of tones and press the button when you hear a tone that is longer than the rest. The long tones are not easy to distinguish, so you must pay close attention.
2. Risks:
   - This is considered to be a minimal risk experiment. You are unlikely to become sick, but you might experience mild motion sickness. (Explain symptoms of motion sickness). We have two way audio communication installed on the device and you will also be monitored at all times on video. If at any time you feel sick, or feel like you want to halt the experiment for any reason, please let us know. (Explain emergency stop)
3. Restraints:
   - You will be restrained in your seat with a hooker harness. It is particularly important that your head does not move during runs. Your head will be situated in a fixed helmet which we must tighten so that your head cannot move within the helmet. To fill any space that your head does not take up, we will pump

up an air bladder that lines the helmet. This may cause some discomfort. If you feel you cannot tolerate the helmet throughout the entirety of the trial, let us know, and we can relieve some air pressure between runs.

4. Runs
   - You will make six 2-minute runs. During the first run you will be rotating in one direction and during the next run you will be rotating in the opposite direction. We will then turn the capsule and perform another two runs, one clockwise and the other counterclockwise. We will turn the capsule again and run the final pair of runs in a similar manner. It takes approximately 10 minutes to turn the capsule. It is during this time that you may opt to bleed the air bladder in the helmet.
5. Any questions?
6. Women- pregnancy test- explain why.
7. Consent form to read and sign.
6. Ask about caffeine/sleep/alcohol/flight in past 24 hrs.

Voluntary Consent to Participate Protocol Number: 30003E

Dates of the Research. From: 12 Jun 95 to 30 Sep 96
Title of Research Protocol: Psychophysical and Neurophysiological Approaches to the Dynamics of Spatial Orientation: Series 2.I.IV: Rotation, High- and Low-G Effects and Effects of Rotating Linear Vectors on Canal-mediated Reactions
Work Unit Number: 061153N MR04101.00F-7303; DN 243516
Principal Investigator/Telephone Number: A. H. Rupert, CDR MSC USN, (904) 452-4496
Medical Monitor/Telephone Number: R. P. Olafson, CAPT MC USN (904) 564-8065

1. You are being asked to volunteer in the research study entitled "Series 2.1.IV. Rotation, High and Low-G Effects: Effects of Direction and Magnitude of Linear Acceleration Vector on Eye Movements and Perception of Spatial Orientation". During your participation in this study you will be involved in the procedures and tests detailed in Attachment A. These experimental procedures are considered to be routine and carry minimal risk and hazard to health.

2. There is a possibility, however, that the procedures may induce the signs and symptoms of motion sickness and that you may have some discomfort from the helmet and restraint system. While in the test enclosure you will be continually monitored by infra-red video cameras and audio communications; you have the option to terminate your participation in the experiment at any time for any reason without prejudice.

3. There is no specific benefit to you as a result of your participation in this study, other than to enhance your awareness of your susceptibility to motion sickness. The research data acquired should enhance scientific knowledge and may be of future benefit to individuals and the Navy mission .

4. Your confidentiality during the study will be ensured by assigning a control number that will be the only identifying entry on any of your research records. The confidentiality of the information related to your participation in this research will be ensured by cross referencing the subject name and control number and maintaining the information in a locked safe by the research staff and will be decoded only when beneficial to the subject or if some circumstance, which is not apparent at this time, would make it clear that decoding would enhance the value of the research data.

5. If you have questions about this study you should contact the following individuals: for questions about research (science) aspects contact A. M. Mead, LT MSC USN at (904) 452-4492 for questions about medical aspects, injury, or any health or safety questions you have about your or any other volunteer's participation, contact R. P. Olafson, CAPT MC USN, Medical Monitor at (904) 452-8065.; for questions about the ethical aspects of this study, your rights as a volunteer, or any problem related to protection of research volunteers, contact R. P. Olafson, CAPT MC USNR, Chair, Committee for the Protection of Human Subjects at (904) 452-8065.

6. Your participation in this study is completely voluntary. If you do not want to participate, there will be no penalty and you will not lose any benefit to which you are otherwise entitled. You may discontinue your participation in this study at any time you choose. If you do stop, there will be no penalty and you will not loose any benefit to which you are otherwise entitled.

7. I have been informed that J. Lloyd is responsible for storage of my consent form and the

research records related to my participation in this study. These records are stored at Bldg. 1811.

8. I have asked the questions on the attached paper, and the written answers provided by the researcher(s) are understandable to me and are satisfactory. I understand what has been explained in this consent form about my participation in this study. I do / do not need further information to make my decision whether or not I want to volunteer to participate. By my signature below, I give my voluntary informed consent to participate in the research as it has been explained to me, and acknowledge receipt of a copy of this form for my own personal records.

Privacy Act Statement

1. Authority. 5 U.S.C. 301

2. Purpose. Medical research information will be collected in an experimental research project entitled Psychophysical and Neurophysiological Approaches to the Dynamics of Spatial Orientation: Series 2.I.IV: Rotation, High- and Low-G Effects and Effects of Rotating Linear Vectors on Canal-mediated Reactions; Work Unit Number: 061153N MR04101.00F-7303; DN 243516 to enhance basic medical knowledge, or to develop tests, procedures, and equipment to improve the diagnosis, treatment, or prevention of illness, injury, or performance impairment.

3. Routine Uses. Medical research information will be used for analysis and reports by the Departments of the Navy and Defense, and other U.S. Government agencies. Use of the information may be granted to non-Government agencies or individuals by the Navy Surgeon General following the provisions of the Freedom of Information Act or contracts and agreements. I voluntarily agree to its disclosure to agencies or individuals identified above and I have been informed that failure to agree to this disclosure may make the research less useful. The "Blanket Routine Uses" that appear at the beginning of the Department of the Navy's compilation of medical data bases also apply to this system.

4. Voluntary Disclosure. Provision of information is voluntary. Failure to provide the requested information may result in failure to be accepted as a research volunteer in an experiment or removal from the program.

_____

Signature of Principal or Associate Investigator, Date (DD/MM/YY)

_____

Signature of Medical Monitor, Date (DD/MM/YY)

_____

Signature of Volunteer, Date (DD/MM/YY)

_____

Signature of Witness, Date (DD/MM/YY)

Voluntary Consent to Participate Attachment A

Protocol Number: 30003E
Dates of the Research. From: 12 Jun 95 to 30 Sep 96
Title of Research Protocol: Psychophysical and Neurophysiological Approaches to the Dynamics of Spatial Orientation: Series 2.I.IV: Rotation, High- and Low-G Effects and Effects of Rotating Linear Vectors on Canal-mediated Reactions
Work Unit Number: 061153N MR04101.00F-7303; DN 243516
Principal Investigator/Telephone Number: A. M. Mead, LT MSC USN, (904) 452-4492
Medical Monitor/Telephone Number: R. P. Olafson, CAPT MC USN
(904) 564-8065
Administration time: 10 minutes.
Questions: You are encouraged to discuss this research with the investigators and medical monitor and to ask questions about medical terms that are not clear to you.

Procedure

In this experiment, you will be seated upright in a chair located in a fixed position about 6 m from the center of rotation of the centrifuge (the NAMRL CAP device). Lateral support to the hips, shoulders and head will be provided and further restraint is afforded by a lap, chest and shoulder harness. You will be in a light-proof enclosure and will be in darkness throughout the centrifuge runs. Your eye movements will be video recorded using infra-red illumination.

The centrifuge motion profile will consist of angular acceleration at 10 deg/s^2 to constant angular velocity of not greater than 104 deg/s which will be maintained for 120 seconds followed by programmed deceleration at 10 deg/s^2 to zero angular velocity. You will remain in a fixed position relative to the centrifuge throughout each run. The seat is always upright (i.e., your head-foot (z) axis is aligned with gravity) and will face in either a forward or backward orientation in an approximately tangential direction (i.e., front-back (x) axis). In one third of the runs, the seat will be aligned with the tangent, while in two thirds of the runs the seat will be fixed so that your x-axis is angled 20 degrees inward or outward from the true tangent. Duration of the entire velocity profile will not exceed 140 s, including the periods of angular acceleration and deceleration. At peak velocity, you will experience a transverse, y-axis, acceleration of not greater than + or - 2.0 G_y, the direction being dependent upon whether you are facing the direction of the motion or have your back to it. The resultant linear acceleration will have a magnitude not exceeding 2.24 G tilted in the roll plane at an angle of up to 63 degrees to your z-axis. The maximum tangential acceleration will be at most + or - 0.1 G

In the experiment, during upramp angular acceleration, you may perceive a circular path of movement and then, after constant angular velocity has been attained, gradual roll up to about 60 degrees of tilt. During deceleration, you may perceive an on-axis turn in the reverse direction and return to upright position.

During each run and for 60 seconds after the CAP stops turning you will be required to perform an audio task in which you have to identify each occasion a long duration tone is presented.

Shortly before the CAP is decelerated you will be asked to make a series of eye movements from side to side in what you perceive to be the horizontal plane. After each run you will be asked to describe your sensations of motion and attitude experienced during the three phases of the run, i.e., during increasing G, at steady G, and during decreasing G.

VITA

Ann Fajardo [redacted]
The daughter of a French mother and a Peruvian father (a Navy physician), Ms. Fajardo has traveled all over the United States and around the world. She received a Bachelor of Science in Engineering Science and Mechanics from Virginia Tech in 1992. She went on to work for the Surface Ship Structural Integrity Group of the Naval Warfare Surface Center - Carderock Division in Bethesda, Maryland until August 1993 when she returned to Virginia Tech to pursue a master of science.

Ann B. Fajardo

REPORT DOCUMENTATION PAGE

Form Approved
OMB No. 0704-0188

Public reporting burden for this collection of information is estimated to average 1 hour per response, including the time for reviewing instructions, searching existing data sources, gathering and maintaining the data needed, and completing and reviewing the collection of information. Send comments regarding this burden estimate or any other aspect of this collection of information, including suggestions for reducing this burden, to Washington Headquarters Services, Directorate for Information Operations and Reports, 1215 Jefferson Davis Highway, Suite 1204, Arlington, VA 22202-4302, and to the Office of Management and Budget, Paperwork Reduction Project (0704-0188), Washington, DC 20503.

1. AGENCY USE ONLY (Leave blank)	2. REPORT DATE	3. REPORT TYPE AND DATES COVERED
	August 1996	Final

4. TITLE AND SUBTITLE

DOES VERGENCE INFLUENCE THE VESTIBULO-OCULAR REFLEX IN HUMAN SUBJECTS ROTATING IN THE DARK?

5. FUNDING NUMBERS

61153N MR04101.00F-7303
61153N MR04101.00G.7405

6. AUTHOR(S)

Ann B. Fajardo

7. PERFORMING ORGANIZATION NAME(S) AND ADDRESS(ES)

Naval Aerospace Medical Research Laboratory
51 Hovey Road
Pensacola, FL 32508-1046

8. PERFORMING ORGANIZATION REPORT NUMBER

Monograph 48

9. SPONSORING/MONITORING AGENCY NAME(S) AND ADDRESS(ES)

Naval Medical Research and Development Command
National Naval Medical Center
Bldg. 1, Tower 12
8901 Wisconsin Avenue
Bethesda, MD 20889-5606

10. SPONSORING/MONITORING AGENCY REPORT NUMBER

11. SUPPLEMENTARY NOTES

Thesis submitted to the Faculty of the Virginia Polytechnic Institute and State University in partial fulfillment of the requirements for the degree of Master of Science in Engineering Mechanics, Blacksburg, Virginia, July 15, 1996.

12a. DISTRIBUTION/AVAILABILITY STATEMENT

Approved for public release; distribution unlimited.

12b. DISTRIBUTION CODE

13. ABSTRACT *(Maximum 200 words)*

In recent experiments involving acceleration stimuli, researchers instructed subjects to focus on a visual target while measuring the vestibulo-ocular reflex (VOR) in one eye. These experiments showed conclusively that the VOR is influenced by target distance. We, on the other hand, were interested in investigating the VOR of subjects accelerated in complete darkness. Specifically, we wished to determine the subject's vergence point, which cannot be accomplished using data obtained from only one eye. Hence, a binocular eye-tracking system that works in the dark was required. In the experiment described in this thesis, the subject was rotated in the dark on NAMRL's Coriolis Acceleration Platform. The position of each pupil center was tracked and recorded by two helmet-mounted infrared cameras connected to a computer-controlled data acquisition system. The position data were used to calculate the angles through which the eyes rotated, and then trigonometric principles were applied to construct the line of sight for each eye for any moment in time; the intersection of these two lines is the vergence point. With the NAMRL binocular eye-tracking system, an accelerating subject's vergence point can accurately be determined if it is less than 1.5 meters away. The vergence data obtained from this experiment suggest that vergence distance does not exclusively drive the VOR in the dark.

14. SUBJECT TERMS

Vergence, vestibulo-ocular reflex, eye movements

15. NUMBER OF PAGES

113

16. PRICE CODE

17. SECURITY CLASSIFICATION OF REPORT	18. SECURITY CLASSIFICATION OF THIS PAGE	19. SECURITY CLASSIFICATION OF ABSTRACT	20. LIMITATION OF ABSTRACT
UNCLASSIFIED	UNCLASSIFIED	UNCLASSIFIED	SAR